ACS APPLIED NANO MATERIALS

www.acsanm.org Article

Ag-Decorated Titania Nanoparticles for Antibacterial Applications

Martina Mercurio,* Farid Hajareh Haghighi, Francesca Ubaldi, Sara Cerra, Maria Luisa Astolfi, Roberto Matassa, Chiara Battocchio, Martina Marsotto, Cinzia De Angelis, Sara Della Monaca, Paola Fattibene, Federica Valeriani, Vincenzo Romano Spica, and Ilaria Fratoddi*

Cite This: https://doi.org/10.1021/acsanm.4c04409 Read Online

ACCESS | Metrics & More | Article Recommendations | Supporting Information

ABSTRACT: In this work, titania nanoparticles (TiO_2NPs) and silver nanoparticles (AgNPs) were combined in situ to obtain a single TiO_2−Ag nanoplatform with synergistic antibacterial effects and perspectives in biological applications. To improve colloidal stability in the aqueous environment, the bifunctional (3-mercaptopropyl)trimethoxysilane (MPTMS) and sodium 3-mercapto-1-propanesulfonate (3MPS) were used as stabilizing agents for covalent binding to TiO_2NP (formation of Ti−O−Si chemical bonds) and AgNP surfaces (through the Ag−S bond), respectively. Synthesis conditions were optimized by tuning the Ag content decorating the TiO_2NPs, and the colloidal stability, size, morphology, and chemical composition were studied in both solution and solid-state by UV−visible, Fourier-transform infrared, ^{1}H NMR, X-ray photoelectron spectroscopy, field emission scanning electron microscopy-energy-dispersive X-ray spectroscopy, transmission electron microscopy, inductively coupled plasma optical emission spectrometry, dynamic light scattering, and ζ-potential. The antibacterial activities of these nanohybrids were investigated on Gram-positive and Gram-negative bacteria, and the results showed an enhanced antibacterial effect arising from the combination of TiO_2NPs and AgNPs in the nanohybrid with the lower Ag content (more than 60% in the case of *S. aureus* exposed to TiO_2−Ag), compared to the pristine TiO_2NPs and control groups. Electron paramagnetic resonance with spin trapping detected the presence of hydroxyl radicals both in the nanohybrids and in the pristine TiO_2NPs, supporting the hypothesis that the antibacterial effect is related to the presence of reactive oxygen species. The results of this research contribute to the synthesis of new potent antimicrobial nanohybrids for applications in more complex biological media.

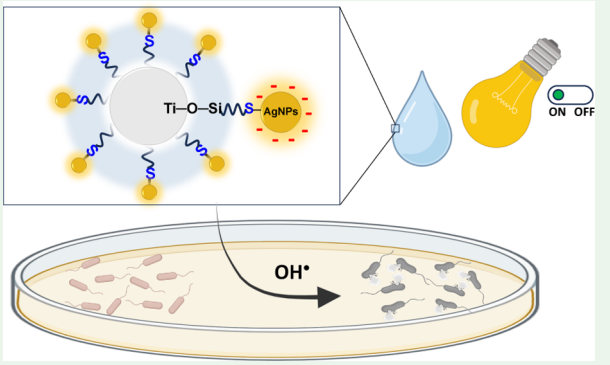

KEYWORDS: *TiO_2 nanoparticles, functionalized AgNPs, hydrophilic nanoparticles, antibacterial activity, E. coli, S. aureus*

1. INTRODUCTION

The widespread overuse of traditional antibiotics has resulted in the emergence of multidrug-resistant bacterial strains and causes serious concerns in different aspects of life such as food safety and human health. In recent years, research on new antimicrobial substances has been focused on metal oxide nanoparticles, particularly TiO_2 nanoparticles (TiO_2NPs), due to their photocatalytic effect, chemical stability, low toxicity, unique physicochemical properties, and cost-effectiveness.[1] Different studies have shown that modified TiO_2NPs can demonstrate excellent antibacterial properties against a broad range of both Gram-positive and Gram-negative bacteria.[2,3] The antibacterial effect of TiO_2NPs is due to their ability to absorb light (UV−vis) and generate reactive oxygen species (ROS), which can be used to damage the chemical structure of microbes.[4−7] This photocatalytic decontamination could be highly effective against bacteria that are now resistant to many conventional antimicrobial agents due to decades of inappropriate antibiotic use.[8]

Similarly, inorganic silver nanoparticles (AgNPs) are known for their potent antibacterial character and, thus, are increasingly used in nanomedicine, consumer products, and water purification to prevent microbial growth.[9] In this regard, AgNPs exhibit different antibacterial mechanisms, including incorporation with the bacteria surface and intracellular uptake (e.g., in *Escherichia coli*) or interaction with sulfur-containing membranes and cytoplasmic proteins to inactivate bacteria.[10] Silver ions (Ag^+) released from AgNPs induce oxidative stress and generate ROS (either in Gram-positive or Gram-negative bacteria), leading to protein dysfunction, membrane, and DNA damage.[11,12] As a member of the noble metal group, AgNPs also possess unique optical (shape and size-dependent surface

Received: July 31, 2024
Revised: August 7, 2024
Accepted: August 9, 2024

plasmon resonance, SPR between 380 and 480 nm)[13,14] and chemical properties that can be combined with the photodynamic−antimicrobial activity of TiO_2NPs for an enhanced effect. Indeed, the combination of AgNPs and TiO_2NPs in a single nanoplatform provides a multifunctional nanohybrid with synergistic effectiveness toward a broader range of bacteria (especially for those resistant to common organic antibacterial agents) or for antibiotics degradation in wastewater treatment.[15−17] Various synthesis methods such as doping,[18] encapsulation in polymers,[19−21] wet chemical impregnation of AgNPs on TiO_2NPs,[22] chemical shell deposition,[23] and TiO_2NPs decoration[24] have been explored. For instance, Soo et al.[25] prepared an $AgTiO_2$ nanocomposite material via electrospinning of a poly(vinylpyrrolidone) (PVP) matrix to easily incorporate both Ag^+ and TiO_2 components homogeneously. Tobaldi et al.[26] prepared Ag^+-doped TiO_2NPs in water/isopropyl alcohol suspension, highlighting that the use of UV-light irradiation in Ag^+-based hybrids leads to a change in the oxidation state of silver ($Ag^+ \rightarrow Ag^0$), although it is necessary to activate TiO_2NPs and achieve an appropriate antibacterial activity. As an alternative, Wang et al.[17] synthesized TiO_2NPs decorated with naked Ag nanoparticles by a photochemical reduction method testing their antibacterial activity against *E. coli* and antibiotics degradation under visible light. Meng et al.[27] proposed an in situ strategy using (3-mercaptopropyl)trimethoxysilane (MPTMS) silane as both stabilizer and reducing agent to promote the formation of AgNPs onto the TiO_2 flat surface, which act as a catalyst for 4-nitrophenol reduction in the presence of sodium borohydride ($NaBH_4$). In this regard, MPTMS acts as a bifunctional silane linker having two different functional groups, e.g.,−SH group and−Si−$(OCH_3)_3$, hydrolyzable in a water/ethanol mixture to form silanol groups (−Si−OH) by a common sol−gel reaction (a modified Stöber method).[28] Then, the condensation reaction occurs between these silanol −Si−OH groups and −OH groups of the TiO_2NPs surface to form the chemical Ti−O−Si bond, releasing methanol molecules.

Herein, we combined and advanced the current state-of-the-art on the preparation of TiO_2−Ag hybrids, proposing a one-pot synthesis procedure in water for titania-silver nanocomposites with different Ag contents. The use of nanostructured counterparts (rather than bulk surfaces) allowed taking advantage of the high surface-to-volume ratio and peculiar nanoscale properties: enhanced the photocatalytic effect of TiO_2NPs and optical plasmonic and antimicrobial properties of AgNPs. Nevertheless, the limited stability in aqueous environments and resistance toward reducing agents (UV-light, chemical reductants) have been addressed via the complete reduction of the Ag^+ precursor in the presence of an additional hydrophilic functionalizing layer around AgNPs, thus broadening the range of applications. Specifically, commercial anatase TiO_2NPs were covalently capped with bifunctional MPTMS silane, followed by in situ nucleation of spherical silver nanoparticles in the presence of the hydrophilic sodium 3-mercapto-1-propanesulfonate (3MPS) thiol as an additional functionalizing layer of AgNPs, achieved by $NaBH_4$ as a reducing agent. The use of 3MPS allowed an increase in the hydrophilicity of the hybrids, making them stable in aqueous environments. The influence of different molar ratios between precursors parameters on the final TiO_2−Ag nanohybrids was studied. The as-obtained TiO_2−Ag colloids were extensively characterized by different advanced techniques, including UV−vis, Fourier-transform infrared (FTIR) [attenuated total reflection (ATR), Far-IR], ^{1}H NMR, field emission scanning electron microscopy-energy-dispersive X-ray spectroscopy (FESEM-EDS), transmission electron microscopy (TEM), inductively coupled plasma optical emission spectrometry (ICP-OES), dynamic light scattering (DLS), ζ-potential, electron paramagnetic resonance (EPR), and X-ray photoelectron spectroscopy (XPS). The evaluation of colloidal stability in ultrapure water and Luria−Bertani (LB) broth over time was important. Antibacterial activity and its stability on multidrug resistance Gram-positive and Gram-negative bacteria were tested, and performances were compared with bare TiO_2NPs and noncovalently PEG-functionalized TiO_2NPs. In this regard, since a possible mechanism for antibacterial activity could be based on the generated ROS during photoirradiation of TiO_2, EPR, combined with spin trapping was used to investigate the generation of hydroxyl radicals both for nanohybrids and the pristine TiO_2NPs. This multimodal, colloidally stable nanohybrid represents a novelty compared with other TiO_2 and silver-based antimicrobial system. The results of this research contribute to the synthesis of new potent antimicrobial nanohybrids with improved stability in different aqueous environments for applications in nanomedicine and biotechnology.

2. EXPERIMENTAL SECTION

2.1. Materials. Titanium(IV) dioxide nanoparticles (TiO_2NPs) (anatase <25 nm, 99.7%), (3-mercaptopropyl)trimethoxysilane [MPTMS: $HS(CH_2)_3Si(OCH_3)_3$, 95%, 196.34 g/mol], silver nitrate ($AgNO_{3(s)}$, ≥99.0%, 169.87 g/mol), sodium 3-mercapto-1-propanesulfonate [3MPS: $HS(CH_2)_3SO_3Na$, 90%, 178.21 g/mol], sodium borohydride ($NaBH_4$, ≥98.0%, 37.83 g/mol), poly(ethylene glycol)-4000 [PEG4000: $H(OCH_2CH_2)_nOH$, 4000 g/mol], tetramethylrhodamine-5-maleimide dye [RHM dye, $C_{28}H_{23}N_3O_5$, ≥85%, 481.50 g/mol], ethanol, and LB broth (Miller) growth powder medium were all purchased from Merck and used without further purification. High-purity nitric acid (HNO_3, 69%) was obtained from Carlo Erba Reagents. Ultrapure water Milli-Q water (H_2O_{up}, resistivity 18.3 MΩ·cm) was supplied by a Zeneer Power I Scholar-UV (Human Corporation) and used for all the experiments involving the aqueous medium. For EPR measurements, high-purity 5,5-dimethyl-pyrroline *N*-oxide (DMPO) (Alexis Vinci Biochem, M.W. 113.2 g/mol) nitrone spin trap was used.

2.2. Silane Functionalization of TiO_2NPs. For the silanization of TiO_2NPs, four reaction parameters, such as time, concentration, solvent, and ammonia catalyst, were investigated in three groups (different TiO_2NPs/MPTMS 1:1, 2:1, 4:1, and 3.5−24 reaction time, presence of the NH_3 catalyst, and solvent, see experimental data reported in Table S1) to obtain well-dispersed nanoparticles with a suitable size. Sample **B4** was selected and used for the synthesis of silver decoration. For this sample, the optimized silanization procedure was as follows: 50 mg of commercial TiO_2NPs were dispersed in 30 mL of solvent (20 mL of ethanol 96% + 10 mL of H_2O_{up}) and sonicated for 5 min. $NH_{3(aq)}$ 37% was injected into the TiO_2NPs colloidal suspension (to adjust the pH at around 8), and then, MPTMS was added to the mixture (25 μL). The mixture was allowed to react at room temperature for 24 h. After the reaction, the TiO_2NPs−MPTMS were separated and purified by centrifugation with fresh H_2O_{up} at 13,400 rpm, +8 °C, and 20 min (3 ×) to remove free MPTMS and byproducts. The amount of available thiols on the TiO_2NPs−MPTMS surface ($C_{-SH\ on\ NPs}$) was determined using eq 1[29]

$$C_{-SHonNPs} = Abs_i - Abs_{surn} \quad (1)$$

where Abs_i is the absorbance of RHM dye stock solution and Abs_{surn} is the absorbance of the supernatant obtained via interpolation of a calibration curve at 545 nm. Further experimental details on RHM-based quantification can be found in the Supporting Information

https://doi.org/10.1021/acsanm.4c04409
ACS Appl. Nano Mater. XXXX, XXX, XXX−XXX

section and Figure S1, together with the synthesis procedure of TiO_2NPs-PEG.

2.3. Synthesis of TiO_2−AgNP Nanohybrids. The synthesis of nanohybrids was carried out by selecting two different TiO_2NPs−MPTMS/$AgNO_3$ weight ratios, i.e., TiO_2NPs−MPTMS/$AgNO_3$ = 4:1 (i.e., 1:0.25, normalized to titania) and 1:2.5 weight ratios, namely, TiO_2−Ag_4 and TiO_2−Ag_1, respectively. In detail, the synthesis was performed in situ by the addition of 20 mg of the TiO_2NPs−MPTMS sample into 5 mL of H_2O_{up} followed by 5 min of sonication. Then, 5 mg or 50 mg (depending on the ratio) of $AgNO_3$ were dissolved in 5 mL of H_2O_{up} and added to TiO_2NPs−MPTMS aqueous suspension. Nucleation of AgNPs onto silanized TiO_2NPs was achieved upon addition of sodium borohydride ($NaBH_4$) in the presence of 3MPS (sodium 3-mercapto-1-propanesulfonate, hydrophilic stabilizer) in $AgNO_3$: 3MPS: $NaBH_4$ = 1:4:10 molar ratio. The mixture was allowed to react under stirring for 2 h at room temperature. The purification process was carried out by ultracentrifugation (13,400 rpm, 20 min, +8 °C), four times for TiO_2−Ag_1 and three times for TiO_2−Ag_4. The reaction was carried out also without adding the 3MPS ligand, obtaining the TiO_2−Ag_4a and TiO_2−Ag_1a samples. The same protocol was used as for the 3MPS-containing nanohybrids.

2.4. Colloidal Stability. The colloidal stability of colloids was studied in ultrapure water and LB broth in the 6.8−7.2 pH range. For each sample, a stock solution at a concentration of 0.2 mg/mL was prepared. Measurements were carried out via UV−vis at regular time intervals (30 min, 1 h, and every 24 h) for 1 week and with DLS within 7 days. Three replicates were performed for each experiment to provide the mean and standard deviation.

2.5. Antibacterial Activity and Stability Studies. The disinfectant activity was tested on Gram-negative *E. coli* (ATCC 25922) and Gram-positive *S. aureus* (ATCC 25923) strains. *E. coli* was cultured on LB broth (LB, Sigma-Aldrich, USA) and *S. aureus* was cultured on Tryptic Soy broth (TSB, Oxoid, Basingstoke, UK). After overnight aerobic incubation at 37 °C, bacteria were recovered over "Brilliance *E. coli*/coliform selective agar" (Oxoid, Detroit, MI, USA) for *E. coli* and "Mannitol Salt Agar" (Oxoid, USA) for *S. aureus*. The *E. coli* and *S. aureus* suspension cultures were then prepared from frozen aliquots of the same stock, rehydrated into fresh LB medium (5% v/v), and incubated overnight at 37 °C until the bacteria reached the stationary growth phase. After incubation, the absorbance of the suspension was measured at 600 nm to determine the bacterial concentration according to calibration curves (DS-11 series spectrophotometer-fluorometer, DeNovix Inc., Wilmington, DE, USA). Therefore, bacterial cells from the same master culture were diluted (about 1:1 v/v) in sterile water to obtain the final bacterial suspension concentration of $(1.0 \pm 0.2) \times 10^4$ and $(1.0 \pm 0.2) \times 10^5$ CFU/mL.

The analyzed nanostructured samples were bare TiO_2NPs, TiO_2NPs−MPTMS, TiO_2NPs−PEG, fresh and aged AgNPs-3MPS, TiO_2−Ag_1 and TiO_2−Ag_4. A comparative test was carried out on the physical mixing of pristine TiO_2NPs and AgNPs-3MPS in the same suspension without any direct covalent linking. Nanostructure samples were redispersed in distilled water at a concentration of 1.1 mg/mL, sonicated using a laboratory sonicator (Vibra-Cell CV 18 SONICS VX 11, Sonics & Materials, CT, USA), vortexed, and diluted up to $1{:}10^9$ v/v.

The specific experimental steps are as follows. Bacterial suspensions (10^4 and 10^5 cells/mL of *E. coli* and *S. aureus*, respectively) were combined with nanohybrids and control samples (1.1, 1.1×10^{-3}, 1.1×10^{-6}, and 1.1×10^{-9} mg/mL) in distilled water. For each sample, 400 μL were transferred to 60 mm Petri dishes and exposed independently at room temperature to white light and in the dark for 25 min. For light exposure, samples were located below the LED system at (14.0 ± 0.5) cm with light emission ranging from 395 to 630 nm in an independent single exposure chamber (isolated by aluminum shields to avoid light contaminations) and open from the front side to ensure identical environmental parameters and external temperature conditions. The temperature of the samples during the illumination was monitored using a Fluke 54 thermocouple thermometer (Everett, Washington, DC, USA) at one-min intervals to exclude significant warming differences and thermic effects. As additional controls, the same samples (treated and not treated) were used, protected by light (in a box or aluminum foil wrapped), in parallel, under the same conditions as the exposed ones. Temperature variations ranged from 22 to 31 °C. After exposure, 100 μL aliquots of each sample were taken and spatulated onto agar plates, and CFU was counted after overnight incubation at 37 °C. Experiments were performed at least in duplicate, and the results were presented as mean ± standard deviation. Data were normalized against the reference control without a photocatalyst. The Student's *t*-test was used for pairwise comparisons. The statistical analyses were performed using SPSS 22.0 (SPSS for Windows; SPSS Inc., IBM, Chicago, IL, USA) at a significance level <0.05. Results were presented in terms of surviving fraction (SF)

$$\%\ \mathrm{SF} = \left(\frac{\text{number of colony}}{\text{control}} \times 100\right)$$

and light activated efficacy (LAE)

$$\%\ \mathrm{LAE} = 100 - \left(\frac{\text{number of colony with light}_{\text{normalized}}}{\text{number of colony with dark}_{\text{normalized}}} \times 100\right)$$

A schematic overview of the microbiological test is reported in Figure S2. To test the antibacterial stability, studies were extended to 30 days under light conditions.

2.6. Spin Trapping EPR Tests. EPR measurements were carried out on a Bruker ELEXSYS E500 spectrometer (Bruker, Germany) operating in continuous wave at the X band, equipped with a high sensitivity Bruker SHQ cavity, at room temperature. The sample was inserted into a glass capillary tube. The light source employed in EPR experiment to stimulate the photocatalytic production of ROS was a 19 W 6500 K LED bulb, set at a distance of 29.2 cm from the sample (power of 1.77 mW/cm^2). An aqueous solution of DMPO (0.1 M) was mixed with an aliquot of TiO_2NPs suspension (volume ratio of 1:1). After 5 min, a 50 μL-aliquot was measured by EPR to get the zero-time point (t_0) in the absence of illumination. A 60 μL aliquot of the same compound was placed in one well of a cell culture plate and exposed to light. The illumination setup is shown in Figure S3. After 2 h of light exposure, a 50 μL aliquot was extracted from the multiwell plate and its EPR spectrum was recorded. The whole procedure was repeated for four aliquots of TiO_2NPs (i.e., four t_0 points and four 2 *h*-points). The t_0 point-aliquots were all stored in the dark after the spectrum recording and then remeasured after 2.5 h. The same experiment was performed with DMPO trapped TiO_2−Ag_1 and TiO_2−Ag_4 nanohybrids and with a DMPO aqueous solution as a control sample.

2.7. Instruments. The UV−vis spectra were recorded using a Varian Cary 100 UV−vis spectrophotometer (wavelength range of 200−800 nm) at room temperature. Quartz cells having a 1 cm optical path length were used.

Particle size $\langle 2R_H \rangle$, nm and size distribution, stability studies, and ζ-potential measurements of the colloidal samples were carried out by DLS technique, using a Malvern Zetasizer Nano-ZS90 with He−Ne red laser at 632.8 nm and an automatic attenuator selection, at 25 °C. Results were performed in triplicate and are expressed as mean ± standard deviation.

FTIR spectra were recorded on a Bruker Vertex 70 instrument in the ATR mode in the 4000−600 cm^{-1} or in transmittance mode in the 4000−400 cm^{-1} range, 32 scans and 4 cm^{-1} resolution. The samples were deposited as solid powders on the sample holder for the ATR mode, as an organic suspension on a thallium bromoiodide (KRS-5) plate for the FTIR mode, or as an aqueous film on a polyethylene plate for far-FTIR. ^{1}H NMR spectra were recorded at 25 °C on a 400.13 MHz Bruker Avance III spectrometer at 9.4 T, in D_2O or $CDCl_3$, and the chemical shift values were given in parts per million (δ, ppm). The acquisition parameters were as follows: 64 k data points, a spectral width of 15 ppm, 64 scans, and a repetition time of 6.55 s to achieve full relaxation for all resonances.

https://doi.org/10.1021/acsanm.4c04409
ACS Appl. Nano Mater. XXXX, XXX, XXX−XXX

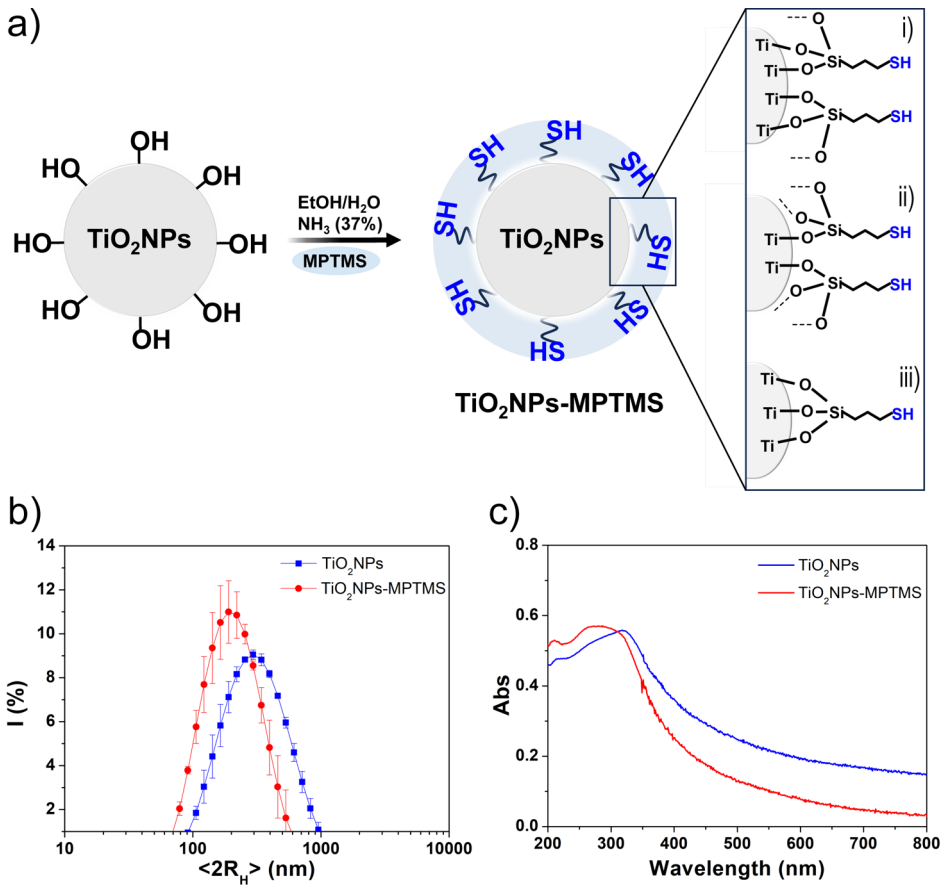

Figure 1. (a) Functionalization scheme of TiO_2NPs surface with MPTMS, varying the silane from (i) and (ii) to (iii) with multibinding modes; (b) UV−vis spectra of bare TiO_2NPs (blue line) and TiO_2NPs−MPTMS (red line) in water; and (c) DLS size distributions of bare TiO_2NPs (blue curve) and TiO_2NPs−MPTMS (red curve) in water.

Inductively coupled plasma optical emission spectrometry (ICP-OES; Vista MPX CCD Simultaneous; Varian, Victoria, Mulgrave, Australia) was used to assess the Ag content in the TiO_2−Ag nanohybrids. The ICP-OES operating parameters were described previously.[30] Three replicates (10 mg each) of the TiO_2−Ag_1 and TiO_2−Ag_4 samples were first digested with concentrated HNO_3 (400 μL, at 80 °C for 30 min). Then, the samples were diluted to a final concentration of 1.0 mg/mL with H_2O_{up} (10 mL) and filtered with a 0.22 μm PVDF syringe filter. As a last step, sample solutions were diluted 1:50 v/v with a 1% HNO_3 (v/v) solution. Yttrium was used as an internal standard at 0.2 mg/L (from 1000 ± 2 mg/L; Panreac Química, Barcelona, Spain). Silver standard solutions (1000 ± 5 mg/L; Merck, Darmstadt, Germany) were prepared for ICP-OES calibration (0.1, 0.5, and 1 mg/L). The following wavelengths (nm) were used: Ag 328.068 and Y 371.029.

The morphology of the nanohybrids was assessed by an Auriga Zeiss field emission scanning electron microscope supported by an EDS detector. The samples were drop-casted from their aqueous colloidal suspensions onto a conductive silicon substrate.[31] TEM images were acquired with a JEOL 2100 LaB TEM operating at 200 kV equipped with an EDS detector.

XPS analysis was performed with a homemade instrument, consisting of preparation and analysis of UHV chambers separated by a gate valve. The analysis chamber is equipped with a six-degree-of freedom manipulator and a 150 mm mean radius hemispherical electron analyzer with a five-lens output system combined with a 16-channel detector giving a total instrument resolution of 1.0 eV as measured at the Ag $3d_{5/2}$ core level. Samples were introduced in the preparation chamber and left outgassed overnight at a base pressure of about 10^{-8} Torr, before introduction in the analysis chamber. Typical vacuum pressure in the analysis chamber during measurements was in the 10^{-8} to 10^{-9} Torr range. The used X-ray radiation is a nonmonochromatized Mg K_α (1253.6 eV). Calibration of the energy scale was made by referencing the spectra to the C 1s core level signal of aliphatic C atoms, found at 285.00 eV, for all samples. Curve-fitting analysis of the C 1s, O 1s, S 2p, Si 2p, Ti 2p, and Ag 3d spectra was performed using Gaussian profiles as fitting functions, after subtraction of a polynomial-type background. S $2p_{3/2,1/2}$ doublets were fitted by using the same full width at half-maximum (fwhm) for each pair of components of the same core level, a spin−orbit splitting of 1.2 eV and a branching ratios S $2p_{3/2}$/S $2p_{1/2}$ = 2/1. Si $2p_{3/2,1/2}$ doublet was fitted as a singlet because of its low spin−orbit splitting. Ti $2p_{3/2,1/2}$ doublets were fitted by using a spin−orbit splitting of 5.8 eV and branching ratios Ti $2p_{3/2}$/Ti $2p_{1/2}$ = 2/1. The Ag $3d_{5/2,3/2}$ doublets were fitted by using the same fwhm for each pair of components of the same core level, a spin−orbit splitting of 6.0 eV and branching ratio Ag $3d_{5/2}$/Ag $3d_{3/2}$ = 3/2. When several different species were identified in a spectrum, the same fwhm value was set for all individual photoemission bands.

3. RESULTS AND DISCUSSION

3.1. Synthesis and Characterization of Functionalized TiO_2NPs. The titania nanoparticle surface functionalization has been carried out in a one-pot silanization process to obtain TiO_2NPs−MPTMS using a condensation reaction to form covalent Ti−O−Si bonds and a silica network around the TiO_2 core, providing a combination of steric and electrostatic stabilizing effect. More importantly, the use of the MPTMS ligand provides the free −SH groups on the TiO_2 surface for further chemical attachment of AgNPs in the nanohybrid. As a

https://doi.org/10.1021/acsanm.4c04409
ACS Appl. Nano Mater. XXXX, XXX, XXX−XXX

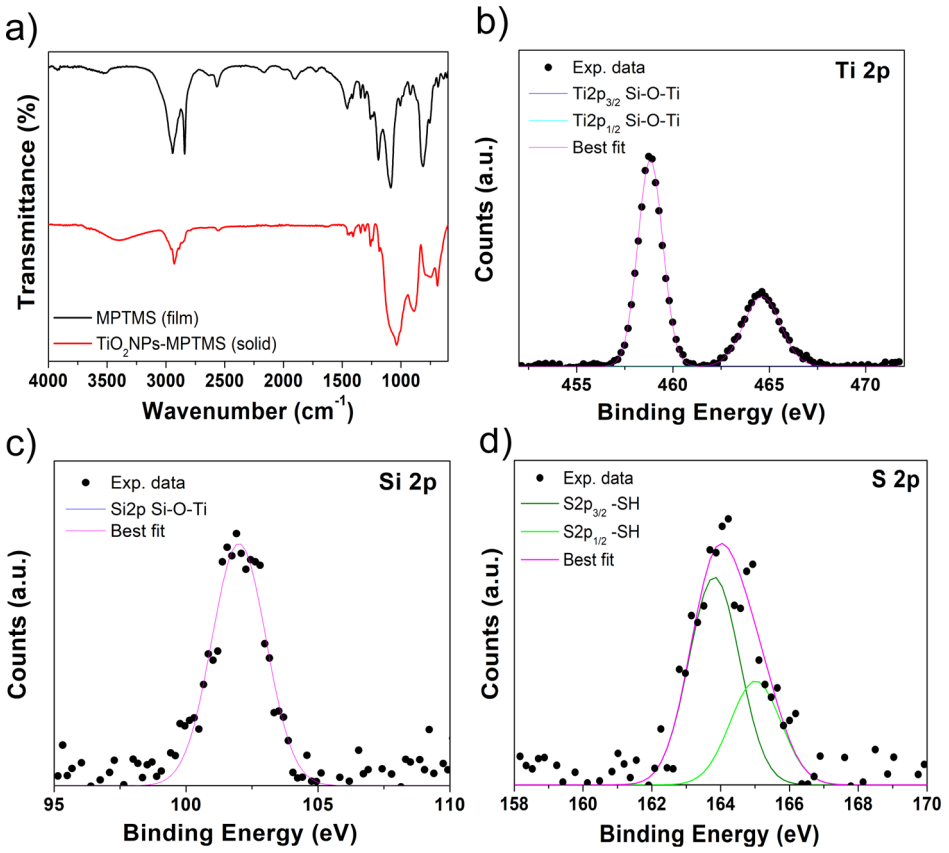

Figure 2. (a) FTIR in the ATR mode of MPTMS (black line) and TiO_2NPs−MPTMS (red line). XPS spectra of TiO_2NPs−MPTMS at (b) Ti 2p, (c) Si 2p, and (d) S 2p core levels.

comparison in the final antimicrobial studies, PEG-functionalized TiO_2NPs were obtained and characterized before use.

3.1.1. Surface Functionalization of TiO_2NPs. Titania nanoparticles covalently functionalized with MPTMS silane were synthesized by a common sol−gel method in a water/ethanol mixture according to the procedure reported in Section 2.2. Formed silanol groups (−Si−OH) can bind to the titania surface in three different modes. Briefly, one, two, or three Si−O−Ti binding modes are possible by varying the concentration of the silane used, as reported in Figure 1a. In (i) and (ii), the Si−O− groups can bind to a vicinal silane grafted on the surface, leading to lateral and vertical polymerization and trapping some of the −SH groups formed within the silica layer, that are not accessible for further conjugation to AgNPs. Thus, appropriate surface silanization occurs in case (iii). Different weight ratios between reagents and conditions were explored (TiO_2NPs/MPTMS 1:1, 2:1, 4:1, reaction time, presence of NH_3 catalyst, Table S1) in order to select the most suitable TiO_2NPs−MPTMS sample for the following silver decoration. Experimental results showed that synthesis in pure ethanol, the absence of NH_3 as a catalyst, and a short reaction time led to aggregated colloids (see Table S1 for full experimental details and main hydrodynamic parameters). Optimum synthesis conditions were found for TiO_2NPs/MPTMS 2:1 weight ratio in water/ethanol 2:1 v/v and in the presence of ammonia solution. Indeed, the latter induces deprotonation of surface −OH groups of TiO_2NPs and fast hydrolysis of the silane, forming a thick stabilizer silica network around the titania core.[3] Thus, sample B4 (hereafter reported as TiO_2NPs−MPTMS) was selected for further studies. To assess the occurred functionalization, a preliminary UV−vis spectrum of TiO_2NPs−MPTMS was recorded and compared with that of bare TiO_2NPs (Figure 1b). Bare TiO_2NPs showed an absorption peak at around 325 nm, attributed to the electronic transition from the valence band (O 2p-based states) to the conduction band (Ti 3d-based states) of their anatase phase.[32,33] As first evidence, the surface silanization of TiO_2NPs induces a 40 nm blueshift to 286 nm in the absorbance maximum with a broadening of the peak.[34,35] A quantification of the surface −SH groups was done via tetramethylrhodamine-5-maleimide (RHM) titration using eq 1 (see Section 2.2 and Figure S1). The number of available thiols was found to be 1.1×10^{19}, equivalent to 1.8×10^{-5} moles of free −SH groups.

Concerning the hydrodynamic size of TiO_2NPs-MPTMS, DLS recorded in water (pH 6.5) showed a single population centered at (210 ± 90) nm, slightly lower than TiO_2NPs before the silanization reaction, which exhibits a hydrodynamic diameter of (295 ± 200) nm (Figure 1c). Moreover, the improved colloidal stability brought by the silane coating was evaluated by measuring the ζ-potential in ultrapure water. For TiO_2NPs−MPTMS, a ζ-potential value of (−30 ± 5) mV was obtained, in contrast with a value of (−15 ± 4) mV of unmodified TiO_2NPs. As known, ζ-potential values ≥ ± 30 mV denote stable colloids in aqueous suspension.[36] To further corroborate the importance of a covalent surface functionalization, noncovalent PEG-functionalized TiO_2NPs were also synthesized for comparison purposes. Specifically, they exhibited higher polydispersity compared with silanized TiO_2NPs with a hydrodynamic distribution of (200 ± 190)

https://doi.org/10.1021/acsanm.4c04409
ACS Appl. Nano Mater. XXXX, XXX, XXX−XXX

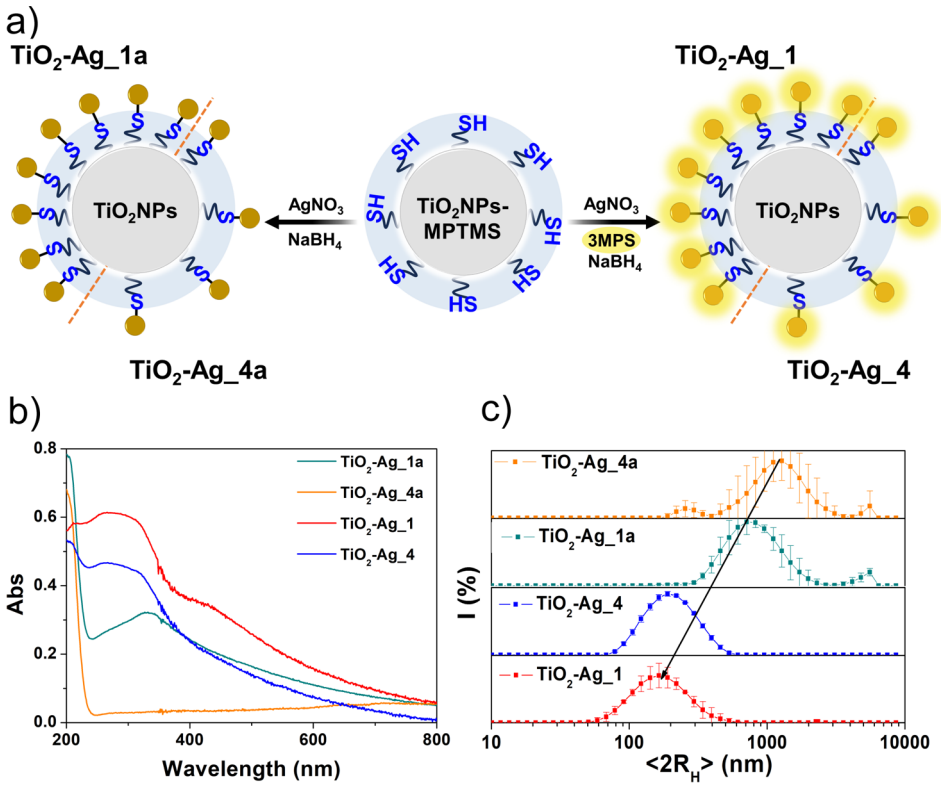

Figure 3. (a) Schematic representation of nanohybrid synthesis used in this work. (b) UV−visible spectra of nanohybrids with 3MPS (TiO_2−Ag_4 and TiO_2−Ag_1) and without 3MPS (TiO_2−Ag_4a and TiO_2−Ag_1a) in water. (c) DLS size distributions of nanohybrids with 3MPS (TiO_2−Ag_4 and TiO_2−Ag_1) and without 3MPS (TiO_2−Ag_4a and TiO_2−Ag_1a) in water.

nm, and a ζ-potential of (−13 ± 3) mV (TiO_2NPs-PEG characterizations are reported in Figure S4). Hence, silanization allowed us to obtain a colloidal titania suspension with a smaller hydrodynamic size distribution and enhanced stability in water toward aggregation (compared with commercial bare TiO_2NPs and TiO_2NPs−PEG), also exploiting surface thiol groups suitable for further Ag decoration.

3.1.2. Surface Characterization of Functionalized TiO_2NPs. Chemical characterization of surface functional groups of TiO_2NPs−MPTMS was carried out via spectroscopic (FTIR and XPS) techniques and ^{1}H NMR. Figure 2a shows the FTIR spectrum recorded in the ATR mode (FTIR−ATR) of MPTMS (black line) overlapped with functionalized TiO_2NPs−MPTMS (red line). ATR spectrum of bare TiO_2NPs taken as a reference is reported in Figure S5. The complete band assignment can be found in Table S2. As can be seen from Figure 2a, following the spectrum of TiO_2NPs−MPTMS, the broad band centered at 3404 cm^{-1} was assigned to a typical stretching (ν) vibration of −OH involved in hydrogen bonds pertaining to TiO_2NPs surface.[37] Vibrational bands at 2930 and 2864 cm^{-1} were due to asymmetric (ν_{as}) and symmetric (ν_s) stretching of $-CH_2$ aliphatic chain of the silane.[37] The peak at 2554 cm^{-1} confirmed the presence of the available thiol moiety on TiO_2NPs. Regarding the other main characteristic bands, they can be found at 1445 cm^{-1} (δ of $-CH_2$, bending), 1345 cm^{-1} ($-CH_2$) deformation modes, 1260 + 1240 cm^{-1} (δ of Si−C, bending), 1184 cm^{-1} stretching (C−O), 1040 cm^{-1} stretching Si−O−Si, 790 cm^{-1} Si−C of aliphatic chain, and 748 (in-plane rocking $-CH_2$).[37,38] The band at 891 cm^{-1} was assigned to stretching Si−O−Ti,[39] whereas the band at 690 cm^{-1} was assigned to Ti−O stretching, which is the characteristic peak of TiO_2.[40] Thus, we assessed the functionalization occurring between MPTMS and TiO_2NPs (−SH detected in the nanoparticles spectrum), via hydrolysis of the methoxy groups from the silane (disappearing of the characteristic $Si-OCH_3$ band in the TiO_2NPs−MPTMS sample, compared with the pristine silane reagent).

Furthermore, the ATR spectra of TiO_2NPs−PEG (Figure S4), clearly showed the presence of characteristic −C−O stretching vibration of PEG at around 1100 cm^{-1}, confirming the presence of the polymer shell around TiO_2NPs.

To further study the interaction of MPTMS with the TiO_2NP surface, the ^{1}H NMR spectrum of TiO_2NPs−MPTMS was recorded, and the result was compared with that of the MPTMS reagent (Figure S5). In the structure of pristine MPTMS ($CDCl_3$), there are five types of protons, including three groups of aliphatic $-CH_2-$ hydrogens, nine methyl hydrogens, and one −SH proton. In the spectrum of free MPTMS, we clearly see all five groups of protons, which appear at around 0.70 ppm [$HS-CH_2-CH_2-\mathbf{CH_2}-Si-(OCH_3)_3$], 1.35 ppm (−SH), 1.80 ppm [$HS-CH_2-\mathbf{CH_2}-CH_2-Si(OCH_3)_3$], 2.50 ppm [$HS-\mathbf{CH_2}-CH_2-CH_2-Si-(OCH_3)_3$], and 3.80 ppm ($-CH_3$) methoxy groups. For TiO_2NPs-MPTMS (Figure S5), an upfield shift for all signals with respect to MPTMS was detected: 0.68 ppm ($HS-CH_2-CH_2-\mathbf{CH_2}-Si-TiO_2$NPs), 1.10 ppm (−SH), 1.63 ppm ($HS-CH_2-\mathbf{CH_2}-CH_2-Si-TiO_2$NPs), and 2.48 ppm ($HS-\mathbf{CH_2}-CH_2-CH_2-Si-TiO_2$NPs). The $-CH_3$ signal was not observed due to the hydrolysis phenomenon, thus further confirming the presence of a functionalizing MPTMS layer around the TiO_2NPs core.

In order to better confirm the MPTMS chemical attachment, XPS analyses were carried out. Complete XPS data (BE,

https://doi.org/10.1021/acsanm.4c04409
ACS Appl. Nano Mater. XXXX, XXX, XXX−XXX

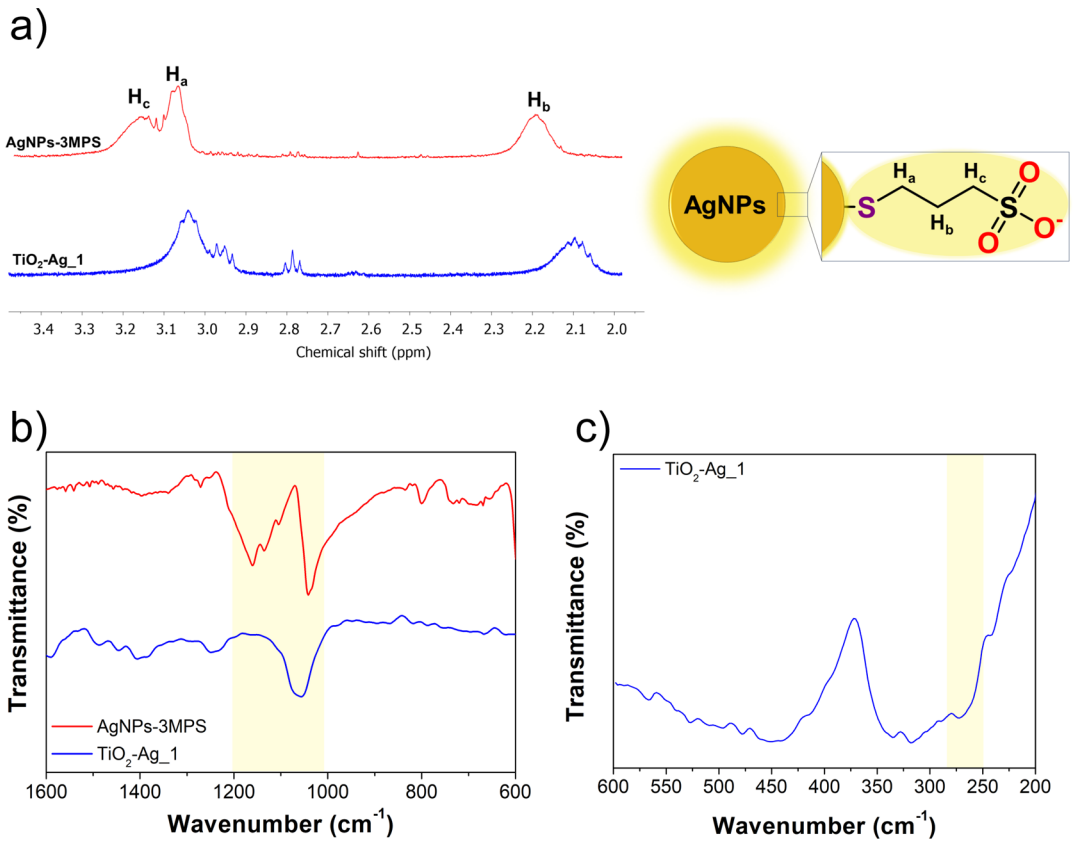

Figure 4. (a) ^{1}H NMR spectra of AgNPs-3MPS (red line) and TiO_2−Ag_1 (blue line) in D_2O. (b) FTIR-ATR spectra of AgNPs-3MPS (red line) and TiO_2−Ag_1 (blue line); (c) Far-FTIR spectrum of the TiO_2−Ag_1 nanohybrid.

fwhm, and assignments) are reported in Table S3. C 1s spectrum of the TiO_2NPs−MPTMS sample appear to be composed of four Gaussian curves (Figure S6). The peak fixed at 285.0 eV is due to the C−C and C−S carbons of the NP functionalities. The peaks at 286.7 and 288.9 eV were attributed to C−O of the NP functionalities and/or of impurity carbons. In particular, the peak of TiO_2NPs−MPTMS at 282.8 eV was mostly due to C−Si bonds of NPs.[41] The Ti $2p_{3/2}$ signal at 458.8 eV (Figure 2b), taken as a reference for the Ti $2p_{3/2-1/2}$ spin−orbit pair, is associated with Si−O−Ti chemical bonds. Ti 2p spectra are made of one spin−orbit doublet (Ti $2p_{3/2}$, Ti $2p_{1/2}$). Si 2p spectrum of TiO_2NPs−MPTMS in Figure 2c was made of one peak at ca. 102.0 eV, which is due to Si−O−Ti, confirming the chemical attachment of Si atoms of MPTMS to the Ti surface.[42] The S 2p spectrum (Figure 2d) was made of a couple of spin−orbit doublet (S $2p_{3/2}$, S $2p_{1/2}$), of which the S $2p_{3/2}$ signal (taken as a reference) around 163.8 eV was assigned to −SH groups of attached MPTMS.[43,44] The O 1s spectrum showed three component peaks (Figure S6). The first, at nearly 530.2 eV, was assigned to the oxygen atoms of TiO_2NPs. The second (BE ca. 531.9 eV) and the third (BE ca. 533.7 eV) were attributed to Si−O−Ti and physisorbed water functionalities, respectively.

3.2. Nanohybrid Synthesis and Characterization. A covalent decoration of TiO_2NPs−MPTMS with AgNPs was carried out in situ by the Ag−S bond, which enhances the permanent loading of AgNPs on the TiO_2 core. The functionalized TiO_2NPs were allowed to react with Ag^+ ions in the presence of 3MPS thiol ligand and a strong reducing agent to form covalently linked TiO_2−Ag_1 and TiO_2−Ag_4 nanohybrids (obtained with different precursors ratio, see Section 2.3).

3.2.1. In Situ Synthesis of TiO_2−Ag Nanohybrids. The procedure of nanohybrid synthesis with different contents is schematically represented in Figure 3a, starting from TiO_2NPs−MPTMS. Our approach was to induce the in situ formation of AgNPs onto the silanized TiO_2NPs surface, starting from the $Ag^+_{(aq)}$ precursor, in the presence of $NaBH_4$ as a strong reducing agent and 3MPS thiol to enhance hydrophilicity and impart colloidal stability to the TiO_2−Ag nanohybrid. In order to tune the surface functionalization, two TiO_2NPs−MPTMS/$AgNO_3$ weight ratios were used, i.e., 4:1 and 1:2.5, to isolate TiO_2−Ag_4 and TiO_2−Ag_1 samples, respectively. For comparison, the nanohybrid was also synthesized without the presence of 3MPS (under the same reaction conditions, see Section 2.3), denoted as TiO_2−Ag_4a and TiO_2−Ag_1a.

The UV−vis spectra of the as-synthesized nanohybrids are shown in Figure 3b. The absence of a 3MPS stabilizing agent led to a partially colloidal aggregation in the case of TiO_2−Ag_4a, in which neither TiO_2NPs nor AgNPs absorption bands arose from the UV−vis spectrum (orange line in Figure 3b). In the case of TiO_2−Ag_1a (dark cyan line in Figure 3b), the typical absorption band of titania nanoparticles was detected, centered at 330 nm, as in the case of 3MPS-functionalized nanohybrid TiO_2−Ag_4 nanohybrid (blue line in Figure 3b), whereas a little-to-no AgNPs SPR band was detected. The absence of the typical plasmonic band on the absorption spectrum can be ascribed to the predominant TiO_2NPs content with respect to the Ag^+ precursor. Indeed, anatase TiO_2NPs show a high absorption coefficient (90 cm^{-1})

https://doi.org/10.1021/acsanm.4c04409
ACS Appl. Nano Mater. XXXX, XXX, XXX−XXX

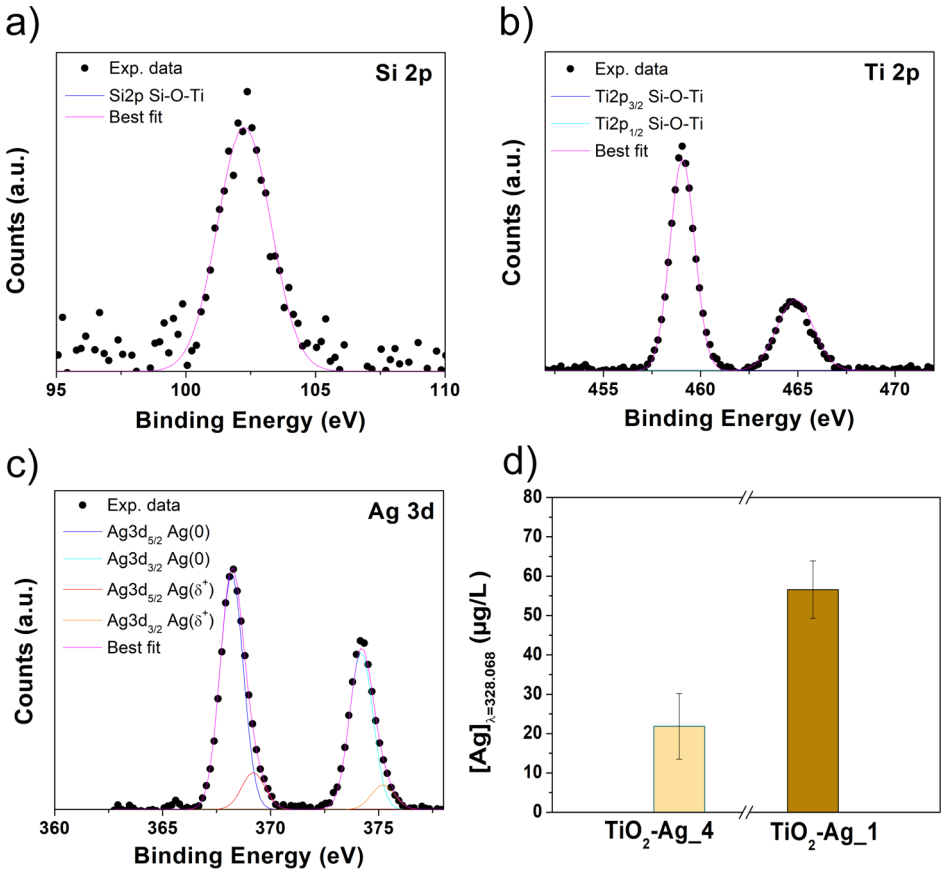

Figure 5. XPS results of TiO_2−Ag_1: (a) Si 2p; (b) Ti 2p; and (c) Ag 3d core levels. (d) ICP−OES results on TiO_2−Ag_4 and TiO_2−Ag_1 samples.

and a high reflective index (ca. 2.5),[45,46] compared with colloidal Ag (within 1.0 to 1.50, depending on the size),[47] which partially overlap with the visible region related to the silver nanoparticles, as reported for similar systems.[48] In the case of the TiO_2−Ag_1 nanohybrid (red line in Figure 3b), a shoulder is detected at around 430 nm, related to the plasmon band of AgNPs together with the broad absorption band centered at about 300 nm due to the titania nanoparticles.

The hydrodynamic behavior of the obtained nanohybrids is compared in Figure 3c. Both TiO_2−Ag_4 and TiO_2−Ag_1 demonstrated a lower hydrodynamic diameter and lower size distribution with respect to the TiO_2NPs−MPTMS precursor (reported in Figure 1c), with $\langle 2R_H \rangle$ values of (190 ± 95) nm and (165 ± 80) nm, for TiO_2−Ag_4 and TiO_2−Ag_1, respectively. Regarding the surface charge, an increase in the stability of the nanohybrids was observed ζ-potential (−28 ± 5) mV and (−38 ± 6) mV, for TiO_2−Ag_4 and TiO_2−Ag_1, respectively. Both of the hydrodynamic results confirm the stabilizing effect of the nanohybrids due to the presence of the 3MPS ligand on the silver surface. A comparison with this reaction was carried out under the same experimental conditions but without adding the 3MPS ligand: TiO_2−Ag_4a with two populations $\langle 2R_H \rangle$ = (1280 ± 510) nm and (255 ± 42) nm with ζ-potential (−27 ± 5) mV, and TiO_2−Ag_1a: single population $\langle 2R_H \rangle$ = (712 ± 356) nm with ζ-potential (−38 ± 5) mV. A large hydrodynamic size was detected in both cases, although they showed good colloidal stability. The ζ-potential has been reported to show a high pH dependence, although an absolute negative charge (ζ-potential of −20 to −55 mV) was also reported for similar TiO_2/Ag nanocomposites.[49] The extensive aggregation in the absence of 3MPS was confirmed by FESEM−EDX analysis (Figure S7). Thus, based on the hydrodynamic size and size distribution (single population, $\langle 2R_H \rangle$ below 200 nm) and good colloidal stability in water (ζ-potential ca. 30 mV), nanohybrids with 3MPS coating TiO_2−Ag_4 and TiO_2−Ag_1 were chosen as suitable candidates for further studies.

3.2.2. Surface Characterization of TiO_2−Ag Nanohybrids. Extensive surface characterization of nanohybrids was carried out via FTIR-ATR, ^{1}H NMR, and XPS, whereas the Ag content was assessed by ICP-OES analysis.

^{1}H NMR spectra of AgNPs-3MPS and the TiO_2−Ag_1 nanohybrid are reported in Figure 4a. In detail, the AgNPs-3MPS exhibited three peaks at δ = 3.23 ppm (AgNPs-S-CH_2−CH_2−$\mathbf{CH_2}$−SO_3^-), δ = 3.17 ppm (AgNPs-S-$\mathbf{CH_2}$-CH_2−CH_2−SO_3^-), and δ = 2.21 ppm (AgNPs-S-CH_2−$\mathbf{CH_2}$−CH_2−SO_3^-). In the nanohybrid TiO_2−Ag_1 spectrum, the proton bonded to the $-SO_3^-$ and −SH moieties underwent an upfield shift, appearing at 3.12 ppm ($\Delta\delta$ = 0.11 ppm) and 3.05 ppm ($\Delta\delta$ = 0.12 ppm), respectively, whereas the $-CH_2$ beta to the −SH was slightly shifted to 2.18 ppm ($\Delta\delta$ = 0.03 ppm), respectively. Regarding the MPTMS ligand on TiO_2−Ag_1, only one signal was detected, corresponding to the proton of $-CH_2$ alpha to the thiol group at 2.87 ppm (see Figure S5). The multiplicity of this signal changes from quartet to triplet, indicating the loss of the proton attached to the thiol group and the absence of unreacted methoxy groups.

FTIR-ATR spectrum of the TiO_2−Ag_1 nanohybrid clearly showed characteristic bands of 3MPS on AgNPs and MPTMS functionalizing TiO_2NPs surface. Full spectra can be found in

https://doi.org/10.1021/acsanm.4c04409
ACS Appl. Nano Mater. XXXX, XXX, XXX−XXX

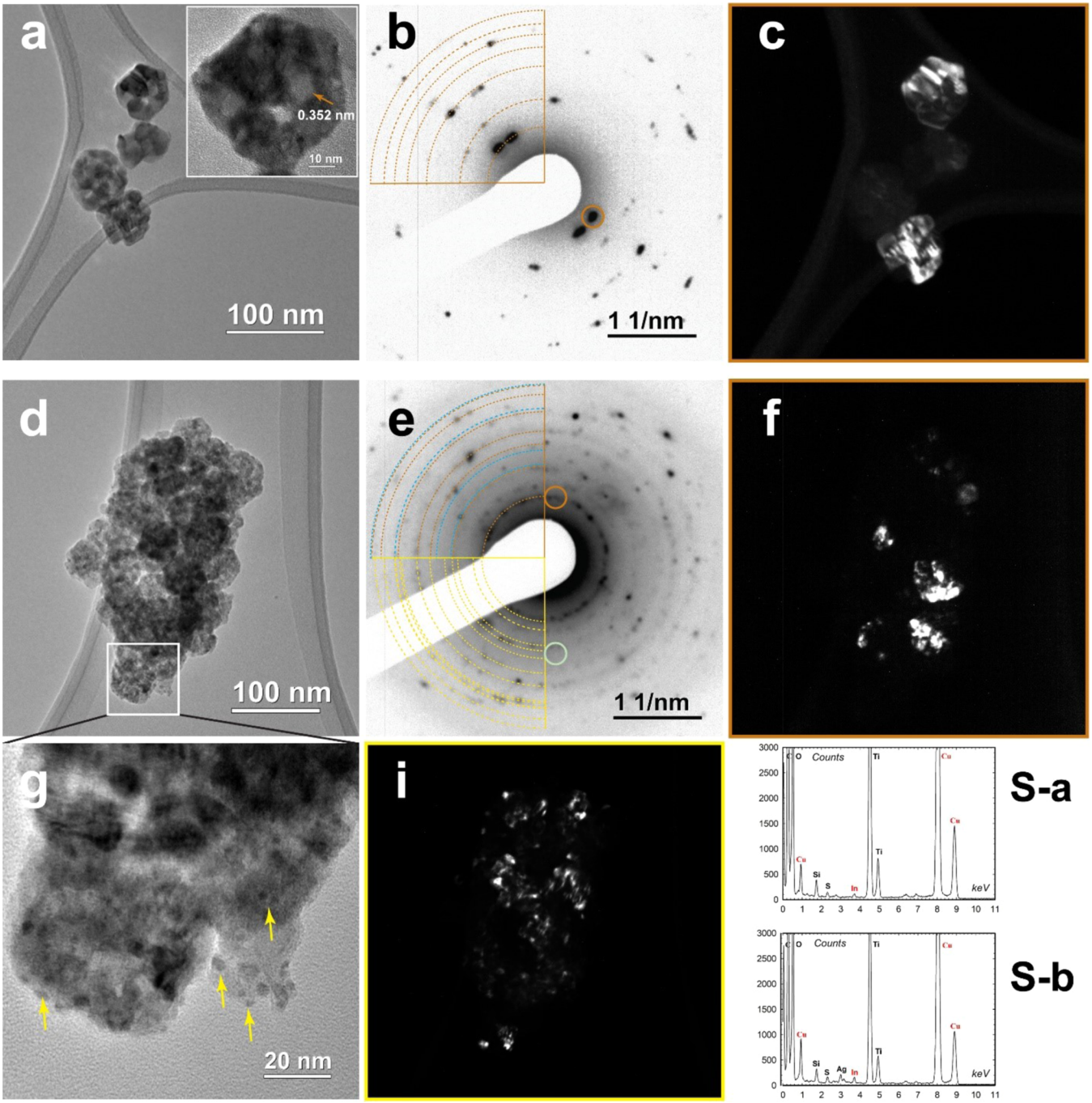

Figure 6. Morpho-structural observation of TiO_2NP−MPTMS: (a) TEM image; (b) EDS spectra; (c) DF image. TiO_2−Ag_1: (d) TEM image, (e) EDS spectra; (f,i) DF image; (g) BF-TEM image; (S-a) TiO_2NPs EDP; and (S-b) TiO_2−Ag_1 EDP.

Figure S8 with their assignments. In Figure 4b, an FTIR in the 1600−600 cm^{-1} wavenumber region is reported. Notably, bands at 1049 and 1131 cm^{-1} are related to ν_s and ν_{as} of $-SO_3^-$ of 3MPS, respectively (highlighted in yellow in Figure 4b), as evidenced from FTIR of AgNPs-3MPS taken as a reference. At 895 cm^{-1}, a signal due to Si−O−Ti vibration was detected, in analogy with pristine TiO_2NPs−MPTMS (FTIR spectra in Figure 2a). The spectrum in the far-IR region (600−200 cm^{-1}) (Figure 4c) allowed us to assess the presence of an absorption centered at 272 cm^{-1}, which is assigned to covalent Ag−S stretching, as reported for similar sulfur-based transition metal complexes (range 298−205 cm^{-1}).[50]

Detailed information about chemical structure of nanohybrids was also obtained via XPS, whereas ICP−OES allowed us to estimate the Ag content. The XPS results of TiO_2−Ag_1 are shown in Figures 5a,b,c and S9. Complete data (BE, fwhm, and assignments) are reported in Table S5.

The signals of C 1s and O 1s that appeared at 282.8 and 531.9 eV were assigned to the C−Si and Si−O−Ti bonds, respectively (Figure S9). The presence of chemical Si−O−Ti bonds was also confirmed in the Si 2p core level spectrum at 102.3 eV (Figure 5a) and in the Ti 2p core level spectrum at 459.1 eV (Figure 5b), consistent with previous reports.[51] S 2p spectra (Figure S9) are made of three couples of spin−orbit doublets (S $2p_{3/2}$, S $2p_{1/2}$) of which the S $2p_{3/2}$ signal is taken

https://doi.org/10.1021/acsanm.4c04409
ACS Appl. Nano Mater. XXXX, XXX, XXX−XXX

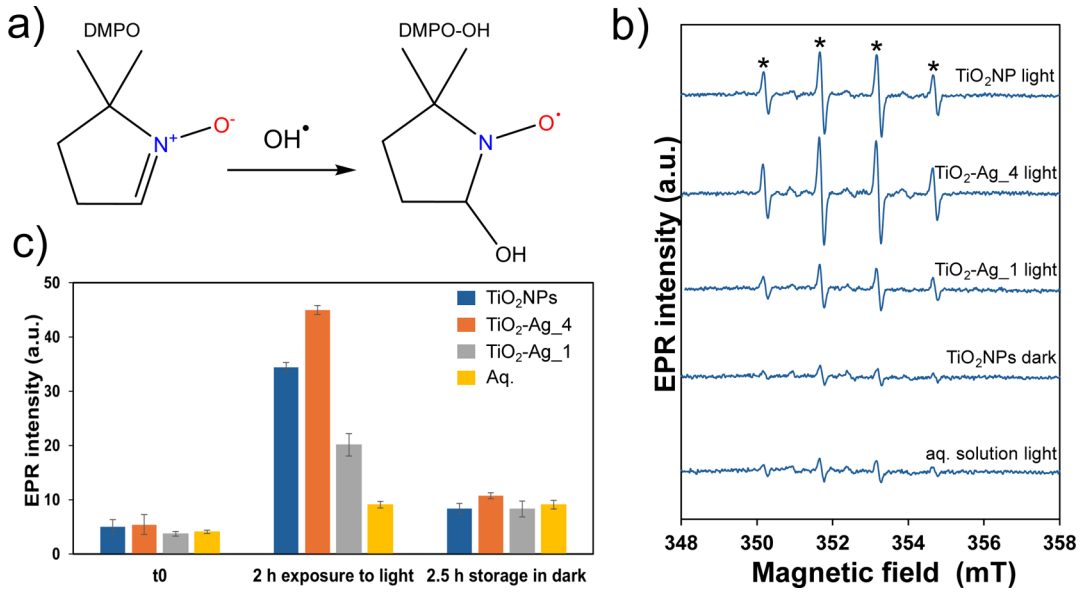

Figure 7. (a) Mechanism of formation of the DMPO−OH• spin adduct and its EPR signal. (b) Signal intensity of the t_0 samples at 5 min, after 2.5 h in the dark, and of the samples illuminated for 2 h. The intensity of each bar is the mean value among four aliquots of the peak-to-peak amplitude of the second line of the DMPO−OH• adducts. The error bars correspond to SD. (c) EPR spectra of TiO_2NPs, TiO_2−Ag_4, and TiO_2−Ag_1 with exposure to light, TiO_2NPs stored in the dark and the spectrum of aqueous solution exposed to light for 2 h. All the spectra were recorded at room temperature; acquisition parameters: 15 mW microwave power; 100 G sweep field; 100 s sweep time; 1 G modulation amplitude; and five scans.

as a reference. S $2p_{3/2}$ signal at around 161.8 eV is relative to sulfurs covalently bonded to the silver nanoparticle surface (S−Ag bond).[52] The S $2p_{3/2}$ signal around 163.2 eV was assigned to thiol-end groups.[43,44] The last component at a higher BE value of 168.4 eV was due to the $-SO_3^-$ moiety of 3MPS. In addition, the formation of silver nanoparticles was confirmed by the Ag 3d spectrum (Figure 5c), showing two pairs of spin−orbit components with the Ag $3d_{5/2}$ peak centered at 368.2 and 369.2 eV for Ag^0 and $Ag^{(\delta+)}$ respectively, coherently with previous results (see Section 3.1.2).

The amount of Ag in TiO_2−Ag_1 and TiO_2−Ag_4 was evaluated by ICP−OES being (57 ± 7) and (22 ± 8) μg/L, respectively (Figure 5d). The herein proposed synthesis method allowed us to modulate the stoichiometry of the final nanohybrids composition.

3.2.3. Morphostructural Characterizations of Pristine TiO_2NPs and TiO_2−Ag Nanohybrids. The solid-state morphology and size of the nanoparticles were evaluated by using FESEM and TEM techniques. Regarding the bare TiO_2NPs, they showed a pH-dependent morphology and size distribution. Based on a previous work,[53] basic pH (≥8) FESEM analysis resulted in grain-like particles with smaller sizes, compared with those at neutral pH (Figure S10). The FESEM image of TiO_2NPs−MPTMS demonstrates a grain-like morphology with a size range of 10−40 nm (Figure S10). These particles are much more homogeneous in terms of size and morphology, compared to the bare TiO_2NPs, due to the stabilizing effect of MPTMS which modulates the shape and size of the TiO_2 core. The EDS spectra confirmed the presence of Ti, Si, C, and S elements, indicating the attachment of the silica layer around the TiO_2NP core (Figure S10).

Morpho-structural TEM observations of dark TiO_2NPs−MPTMS strictly linked to each other, forming polygonal nanostructured particles of about 68 nm in size, are shown in Figure 6a. At high TEM magnification, visible crystalline lattice fringes with spacing d = 0.352 nm are shown in the corresponding inset of Figure 6a, due to the (101) plane of the TiO_2 anatase phase.[54] This atomic and structural compositions of the observed aggregate have been confirmed by EDS and electron diffraction pattern (EDP) and are shown in Figure 6b,S-a. The EDS spectrum evidences the high purity of the aggregates, showing intense peaks belonging to Ti species (Cu and In peaks are from the support grid and TEM). The silicon and small sulfur peaks can be ascribed to the presence of the MPTMS ligand linked on the TiO_2NPs surface. The experimental diffraction spots, ascribable to the presence of a single crystal, have been reproduced by EDP, simulated by considering the with *I41/amdZ* tetragonal symmetry.[55] To visualize the spatial distribution of the crystalline phase detected by EDP, we used dark field (DF) imaging. DF images have been obtained by placing the objective aperture around a diffracted beam of the EDP of region I (brown circle of Figure 6b), corresponding to the arc of the (101) Debye ring. DF image proves that the nanometric anatase crystals are present in the polygonal NPs (Figure 6c).

The TiO_2−Ag_1 nanohybrid has been characterized by polygonal nanoparticles of about 49 nm in size still observed in the TEM image of Figure 6d. The TEM image of TiO_2−Ag_1 shows two main regions having different contrasts, including gray and black portions attributed to the AgNPs and TiO_2NPs, respectively (Figure 6d,g). The corresponding EDP exhibits diffraction rings produced by random orientation of the polycrystalline material (Figure 6e). By measuring the *d*-spacing of the diffraction rings, we were able to identify a superimposition of three different diffraction patterns. The strong signal of the diffraction rings indicated by brown arcs belongs to the TiO_2 crystallites detected before (Figure 6b), confirmed also by the intensive ring of d_{101} = 0.349 nm. The second EDP has been identified by considering the crystalline phase of silver sulfide (Ag_2S).[56] The calculated *d*-spacing of a monoclinic space group P21/n well matched with our experimental interplanar spacing of the diffraction rings

https://doi.org/10.1021/acsanm.4c04409
ACS Appl. Nano Mater. XXXX, XXX, XXX−XXX

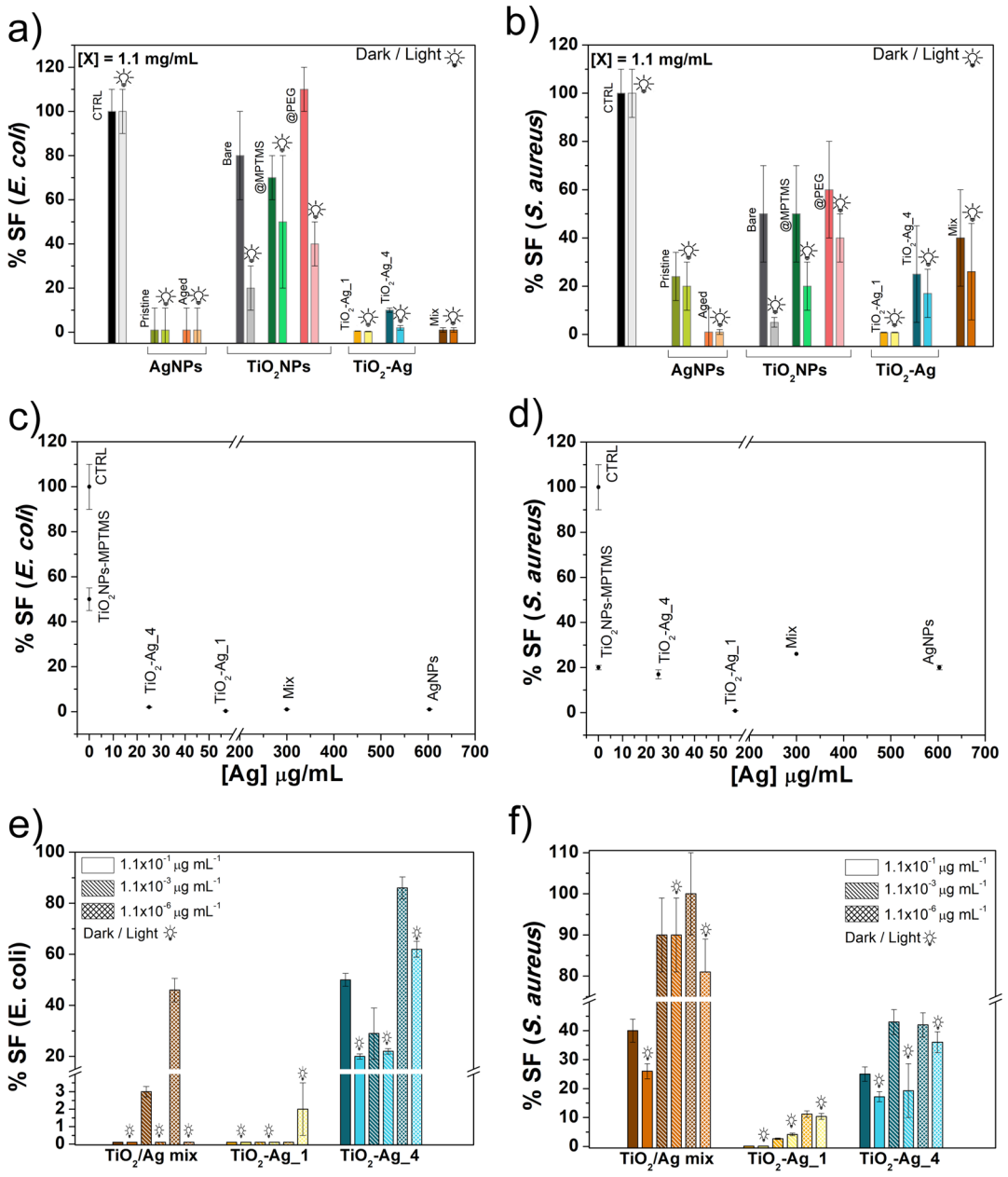

Figure 8. Antibacterial tests on pristine and aged AgNPs, bare, MPTMS, and PEG stabilized TiO_2NPs, and TiO_2−Ag_4 and TiO_2−Ag_1 nanohybrids compared with TiO_2NPs/AgNPs physical mix: *E. coli* tests: (a) SF (% SF) in dark and light conditions, (c) SF (% SF) at different Ag concentrations toward *E. coli*, and (e) SF (% SF) at different concentrations (1.1×10^{-1}, 1.1×10^{-3}, and 1.1×10^{-6} $\mu g\ mL^{-1}$); *S. aureus* tests: (b)% SF (% SF) in dark and light conditions, (d) SF (% SF) at different Ag concentrations toward *S. aureus*, and (f) SF (% SF) at different concentrations (1.1×10^{-1}, 1.1×10^{-3}, and 1.1×10^{-6} $\mu g\ mL^{-1}$).

(yellow arcs), in which the measured and calculated highest intensity signals belong to the (−111) diffraction plane with an interplanar spacing of d_{-111} = 0.344 nm. The blue arcs evidence the presence of pure silver nanoparticles with a face-centered cubic (fcc) structure. The corresponding DF images evidence both presences of TiO_2NPs and AgNPs with the Ag_2S shell (Figure 6f,i). Moreover, the high magnification BF-TEM image of Figure 6g shows dark nanoparticles, as indicated by yellow arrow, that can be attributed to the silver nanoparticles confirmed by EDS by which the silver contribution is shown in the spectrum of Figure 6S-b.

3.2.4. EPR Measurements. EPR/spin trapping analysis was used to analyze the generation of hydroxyl radicals, through the analysis of the formation of a DMPO−hydroxyl radical spin adduct (whose mechanism is illustrated in Figure 7a).[57] In Figure 7b, the results of the experiment for the investigation of the hydroxyl generation for the TiO_2NPs, the TiO_2−Ag_1 and TiO_2−Ag_4 nanohybrids, and the DMPO aqueous solution are shown. For each sample, the signal intensities of the t_0 sample at 5 min and at 2.5 h and of the samples exposed to light for 2 h are reported. The intensity of each bar corresponds to the mean value among four aliquots of the peak-to-peak amplitude of the second line of the DMPO−$OH^{\bullet}$ adducts. The error bars correspond to the SD. The spectrum line amplitude is linked to the number of $OH^{\bullet}$ present in the solution.

In Figure 7c, the spectra of TiO_2NPs, TiO_2−Ag_4 and TiO_2−Ag_1 nanohybrids and DMPO aqueous solution at t_0,

https://doi.org/10.1021/acsanm.4c04409
ACS Appl. Nano Mater. XXXX, XXX, XXX−XXX

after 2 h exposure to light and after 2.5 h storage in dark are shown. The typical four-line EPR spectrum (indicated by asterisks) of the DMPO−$OH^{\bullet}$ adduct is evident in all five spectra. The EPR spectrum showed no changes in line shape, which excluded the generation of radicals other than $OH^{\bullet}$ in all samples. The spectrum line amplitude of the samples stored in dark for 2.5 h was on average a factor (2.2 ± 0.3) higher than in the samples measured at t_0, indicating a similar spontaneous generation of radicals in all samples when non exposed to light. In the samples exposed to light for 2 h the signal amplitude was higher than in the t_0 sample by a factor (6.8 ± 1.8) for TiO_2, 8,3 ± 2.8 for TiO_2−Ag_4, and (5.4 ± 0.6) for TiO_2−Ag_1. Therefore, more radicals were formed in the presence of light than in it, an effect likely linked to photocatalysis. Moreover, the hydroxyl radical concentration was higher for TiO_2−Ag_4 and lower for TiO_2−Ag_1 when compared to TiO_2.

3.3. Antibacterial Studies. *3.3.1. Antibacterial Activity Evaluation on E. coli and S. Aureus.* In this study, the synergic effect of TiO_2 with AgNPs was analyzed, with the aim of studying the effects for photocatalytic disinfection processes. The impact on *E. coli* (Gram-negative) and *S. aureus* (Gram-positive) strain targets was studied by assessing the single component response to the efficacy of nanohybrids. Freshly prepared and aged AgNPs suspensions, commercial bare TiO_2NPs, and TiO_2NPs−MPTMS and TiO_2NPs−PEG samples were compared to TiO_2−Ag_4, and TiO_2−Ag_1 nanohybrids and the physical TiO_2NPs/AgNPs mix. Studies were carried out in the dark and exposed to white light for 25 min.

In Figure 8a, the normalized surviving fraction, SF (%), in the presence of the *E. coli* strain was reported and compared with the experiments in the presence of *S. aureus* in Figure 8b, in contact with nanostructured samples at 1.1 mg/mL (in distilled water). The antimicrobial activities toward *E. coli* of both pristine and aged AgNPs and of the physical TiO_2NPs−AgNPs mix were effective, with a SF less than 1% in both dark- and light-exposed samples, with no relevant effect due to light. On the other hand, bare TiO_2NPs showed a marked photocatalytic effect, with a SF under light of about 20%. When chemically or physically surrounded by a stabilizing agent, the photocatalytic effect and antimicrobial activity were less effective, with a lower activity in light conditions: around 50% for TiO_2NPs−MTPMS and 40% for TiO_2NPs−PEG samples. Both nanohybrids showed a marked response as well as the physical TiO_2NPs/AgNPs mix with a comparable response, and a slight photocatalytic effect for TiO_2−Ag_4. When studying the SF of *S. aureus* (Figure 8b), it is possible to observe a different behavior that should be considered in the higher resistance of this Gram-positive strain. The functionalized AgNPs-3MPS samples resulted effective, with a SF of about 20% and less than 1% for pristine and aged samples, respectively, in both dark and light conditions. The titania-based samples showed a marked photocatalytic effect and SF values of 5, 20, and 40% for bare TiO_2NPs, @MPTMS, and @PEG functionalized samples, respectively. In the case of the hybrids, the TiO_2−Ag_1 sample was more effective (SF less than 1% either with and without light irradiation) with respect to TiO_2−Ag_4 (SF 25% in the dark and 17% upon light irradiation). By comparison with the physical TiO_2NPs−AgNPs mix (SF 40% in the dark and 26% upon light irradiation), the TiO_2−Ag_4 sample was more effective, showing not only the important role of silver for antibacterial applications but also a synergistic antibacterial/photocatalytic effect due to the presence of titania nanoparticles in the latter sample.

The effect of light was calculated by the LAE% (see Section 2.5 and Figure S11). It was possible to observe that the TiO_2−Ag_4 sample showed a prominent LAE with respect to other samples of about 80 and 83%, for *E. coli* and *S. aureus*, respectively. This behavior was ascribed to a higher hydroxyl radical concentration generated by TiO_2−Ag_4 compared with that of TiO_2−Ag_1, as demonstrated by EPR measurements (see Section 3.2.4).

In Figure 8c,d, the antibacterial activity was studied considering the different Ag concentrations, previously calculated by ICP−OES analysis (see Section 3.2.2). In the case of *E. coli*, TiO_2−Ag_4, TiO_2−Ag_1, AgNPs-3MPS, and the physical mix, appear to have similar performances, although the difference in silver content among these samples, should be considered: (57 ± 7) μg/mL and (25 ± 8) μg/mL for TiO_2−Ag_1 and TiO_2−Ag_4 nanohybrids, respectively, compared to (300 ± 5) μg/mL for TiO_2NPs/AgNPs physical mix, and (603 ± 10) μg/mL for pristine/aged AgNPs-3MPS. This result suggests that the nanohybrids show higher antibacterial performance compared to the physical mix and AgNPs-3MPS with a significantly lower silver concentration. Also, in the case of *S. aureus* (Figure 8d), effective antibacterial activity was optimized in the nanohybrids, with the best efficacy for the TiO_2−Ag_1 sample. For *E. coli*, approximately 100% cell death was achieved in the presence of Ag in the range of (25−603) μg/mL, whereas for *S. aureus*, 57 μg/mL of Ag is needed to achieve the same results. However, being aware of the greater resistance of Gram-positive bacteria like *S. aureus* to silver nanoparticles than that of Gram-negative bacteria,[58] a remarkable antibacterial effect toward *S. aureus* was achieved by the TiO_2−Ag_1 nanohybrid in the form of AgNPs chemically bound to the nanostructured titania producing a synergistic antibacterial effect even in the dark. These results underscore the synergistic effect achieved in a single nano-platform due to the covalent combination of the intrinsic photocatalytic effect arising from titania (formation of hydroxyl radicals) and the effective antimicrobial activity shown by AgNPs.

In Figure 8e,f, the antibacterial activity of the nanohybrids was compared to that of the physical mix by varying the sample concentration from 1.1×10^{-1} to 1.1×10^{-6} mg/mL, corresponding to an Ag content ranging from 330×10^{-1} to 25×10^{-6} μg/mL. In the case of the *E. coli* strain (Figure 8e), the TiO_2−Ag_1 nanohybrid exhibited high antibacterial activity, resulting in complete bacterial colony eradication even in the absence of light exposure when diluted up to 1.1×10^{-6} mg/mL with distilled water. The TiO_2−Ag_4 sample is less effective with respect to TiO_2−Ag_1 and the results are clearly dependent on the applied dose and silver content, with light-dependent antibacterial activity at all dilutions tested. The physical mix was highly effective, achieving up to 100% cell death within the 1.1×10^{-1} to 1.1×10^{-3} mg/mL range. However, it contained about 5 times more silver than TiO_2−Ag_1, and it lost efficacy with dilution, with a pronounced light-dependent effect.

In the case of *S. aureus* (Figure 8f), the TiO_2−Ag_1 nanohybrid maintained the antibacterial activity upon dilution, also at concentration 1.1×10^{-6} mg/mL, containing 57×10^{-6} μg/mL Ag content, without significative light-dependent effect at higher dilution. On the other hand, TiO_2−Ag_4 nanohybrid was less effective than TiO_2−Ag_1, showing a %SF about 35%

https://doi.org/10.1021/acsanm.4c04409
ACS Appl. Nano Mater. XXXX, XXX, XXX−XXX

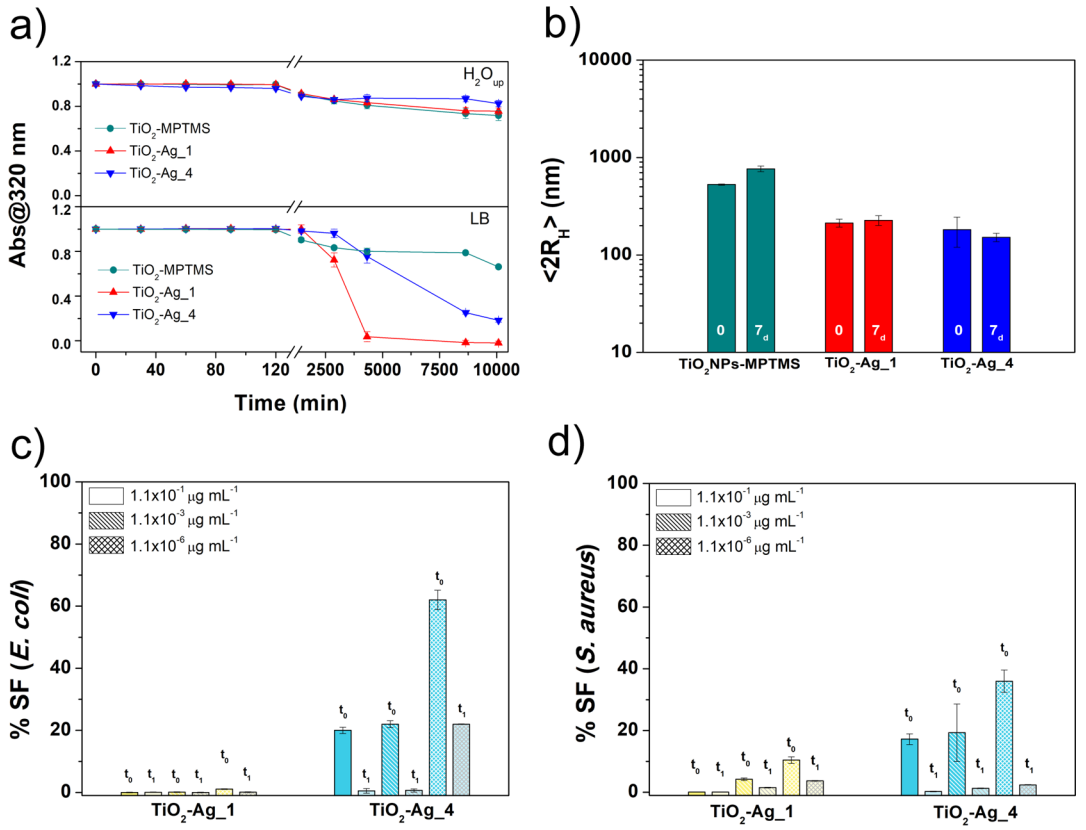

Figure 9. (a) Colloidal stability monitored by UV−vis absorbance at 320 nm of TiO_2NPs-MPTMS (dark cyan), TiO_2−Ag_1 nanohybrid (red line), and TiO_2−Ag_4 nanohybrid (blue line). The concentration of colloids was 0.2 mg/mL measured in H_2O_{up} and in LB broth; (b) DLS hydrodynamic size histogram for TiO_2NPs-MPTMS (dark cyan), TiO_2−Ag_1 nanohybrid (red), and TiO_2−Ag_4 (blue) colloidal samples measured at t = 0 and t = 7 days. Antibacterial stability (t_0 = after 25 min light irradiation; t_1 = after 1 month) as a function of different concentrations of TiO_2−Ag_1 and TiO_2−Ag_4; (c) tests in the presence of *E. coli*; and (d) test in the presence of *S. aureus*.

upon light irradiation at concentration 1.1×10^{-6} mg/mL containing 25×10^{-6} μg/mL Ag content, whereas TiO_2NPs/AgNPs completely lost efficacy as early as the 10^{-3} dilution.

These results demonstrated that nanohybrids, characterized by covalent bonding between titania and silver nanoparticles, are highly effective even at extremely high dilutions with very low Ag content, compared with other studies. For instance, V.T. Nguyen et al. achieved notable antibacterial activity against *E. coli* and *S. aureus* with a 40 mg/mL Ti−Ag nanohybrid containing 1.3 mg/mL AgNPs, showing dark and light inhibition zones.[59] M.V. Lungu et al. showed how the antibacterial activity increased with the increasing of AgNPs content, obtaining the most active nanocomposite with 2.34 wt % AgNPs, being more effective for Gram-positive bacteria.[60] Zhang. et al. synthesized TiO_2−Ag nanohybrids via room-temperature ionic liquids with four different Ag concentrations (1.2, 2.4, 3.0, and 3.6 μg/mL) and observed complete *E. coli* inhibition at 2.4 μg/mL of Ag content after 20 min of exposure.[61]

Considering the minimum concentration used for TiO_2−Ag_1 and TiO_2−Ag_4 nanohybrids (1.1×10^{-6} mg/mL, with Ag contents of 57×10^{-6} and 25×10^{-6} mg/mL, respectively), a potent antibacterial activity is observed on both *E. coli* and *S. aureus*, which has been rarely reported in literature for other types of TiO_2−Ag nanohybrids, demonstrating the effectiveness and importance of this conjugation strategy through the MPTMS bifunctional linker for preparing the advanced nanoantibacterials. Compared to the previous works, the observed antibacterial effect of TiO_2−Ag_1 and TiO_2−Ag_4 is related to their unique chemical structure in which both antibacterial TiO_2NPs and AgNPs-3MPS are chemically linked together with a specific distance from each other (because of the MPTMS layer). This structure allows both TiO_2- and AgNPs to exhibit their antibacterial properties through different mechanisms within a single nanoplatform, resulting in a highly significant synergic effect. In fact, this chemical structure provides locally concentrated antibacterial species (ROS, Ag^+, etc.) derived from the nanohybrids. The selected MPTMS and 3MPS layers decrease the agglomeration of the nanocomponents, which enhances the bactericidal effect of this new system.

3.3.2. Colloidal and Antibacterial Stability over Time. Colloidal stability of nanoparticles is a key factor for their potential biological applications and directly affects their effectiveness. The stability in suspension was evaluated following the absorbance of TiO_2NPs−MPTMS, TiO_2−Ag_1 nanohybrid, and TiO_2−Ag_4 nanohybrid colloids at 320 nm (absorption maximum of TiO_2NPs) in two different media (0−7 days) with similar pH (6.8−7.2) but different ionic strengths: ultrapure water (negligible ionic strength) and LB broth (LB ca. 170 mM, Figure 9a). Concerning the colloidal stability in water (Figure 9a), samples showed a high stability within 2 h; then, they started to sediment (10% after 24 h) up to 30% sedimentation after 7 days. In the LB broth (Figure 9a), a different behavior was detected among samples: MPTMS-functionalized TiO_2NPs and nanohybrids followed

https://doi.org/10.1021/acsanm.4c04409
ACS Appl. Nano Mater. XXXX, XXX, XXX−XXX

a trend comparable with the water environment, i.e., stability over precipitation within 2 h. TiO_2NPs−MPMTS and TiO_2−Ag_1 started to sediment by about 20% after several minutes, reaching approximately 100% after 7 days. A prolonged stability was detected for TiO_2−Ag_4, which precipitated by ca. 10% after 2 h up to 35% within a week. To further evaluate the sedimentation process, studies in LB broth were extended on hydrodynamic diameter evolution over time. In Figure 9b, hydrodynamic values taken at t = 0 and t = 7 days were reported.

As first evidence, all samples showed good stability over 7 days, with a $\langle 2R_H \rangle$ of about 200 nm for TiO_2−Ag_1 and TiO_2−Ag_4, whereas a higher hydrodynamic value was found in the case of TiO_2NPs−MPTMS (ca. 500 nm). Within a week, values were retained in all cases, with a slight increase for TiO_2NPs−MPTMS (up to 700 nm).

The appearance of a larger populations (>500 nm) in the LB medium, compared to single size distributions previously detected in water (see Section 3.2.1), can be attributed to the higher ionic strength, reported to cause aggregates formation in similar functionalized hydrophilic silver nanoparticles.[62] The instability was explained on the basis of the reduction of the electrical double layer around NPs core enhancing the particle−particle interaction.[62] Conversely, TiO_2−Ag_1 showed better stability toward formation of aggregated fractions probably due to the presence of a higher 3MPS functionalizing layer around AgNPs, as expected on the basis of the experimental procedure (higher amount of 3MPS used). In all cases, hydrodynamic size was retained over time, allowing to conclude that sedimentation process early detected by UV−vis was due to simple flocculation and not driven by irreversible colloidal aggregation.

The antibacterial stability of the TiO_2−Ag_1 and TiO_2−Ag_4 nanohybrids with concentration in the range 1.1×10^{-1} to 1.1×10^{-6} mg/mL was also investigated to assess the long-term activity against *E. coli* and *S. aureus* comparing the SF % data at t_0 (after 25 min light irradiation) and t_1 (after 1 month). In the case of *E. coli* (Figure 9c), the TiO_2−Ag_1 nanohybrid maintained the antibacterial activity over time and also upon dilution, assuring a very effective and stable bacterial colony eradication. The efficacy of the TiO_2−Ag_4 nanohybrid improved with time, even at high dilution with a SF % equal to 22% in the sample at concentration 1.1×10^{-6} mg/mL. As a comparison, the TiO_2−Ag_4 nanohybrid (Figure 9d) shows a similar trend with a more effective efficacy and antibacterial stability after 1 month. As a result, colloidal and antibacterial stability of the nanohybrids exhibit great long-term performances.

4. CONCLUSIONS

In this work, novel nanohybrids based on the covalent combination of MPTMS-functionalized TiO_2NPs and 3MPS-functionalized AgNPs were synthesized via wet chemical reduction using sodium borohydride in water. The MPTMS bifunctional ligand allowed the improvement of the colloidal stability of titania nanoparticles and the decoration of them with different contents of in situ prepared AgNPs through a proper choice of synthesis parameters. Hydrophilic AgNPs-decorated TiO_2 nanoparticles were isolated and extensively characterized with both spectroscopic and morphological techniques to assess their size, size distribution, shape, covalent Ti−O−Si and Ag−S surface functionalization, and high colloidal stability (in water and LB broth) within 7 days. The antibacterial activity was investigated on *E. coli* and *S. aureus* bacteria, comparing performances under light irradiation (light emission ranging from 395 to 630 nm, 25 min exposure) and in the dark. A superior antibacterial effect was observed in the case of nanohybrid samples with respect to bare and noncovalently functionalized TiO_2NPs and control groups. The nanohybrids showed an enhanced antimicrobial activity with respect to the physical mix, with an SF = 2% in the presence of *E. coli* and 10% in the presence of *S. aureus*, at 1.1×10^{-6} μg/mL, despite the low Ag content (57×10^{-6} μg/mL). Both nanohybrids showed high antibacterial stability over 1 month. A different behavior was observed according to the surface functionalization of TiO_2NPs under different light/dark conditions. The lower the Ag decoration, the higher the photocatalytic response under light irradiation due to higher hydroxyl radical generation, as evidenced by EPR analysis. The decorated TiO_2−Ag nanohybrids as a multimodal, colloidally stable system represents a novelty compared with similar TiO_2 and silver-based antimicrobial systems, opening perspectives in public health and environmental remediation.

■ ASSOCIATED CONTENT

Supporting Information

The Supporting Information is available free of charge at https://pubs.acs.org/doi/10.1021/acsanm.4c04409.

Determination of free thiol groups on TiO_2NPs-MPTMS with RHM dye; PEGylation of TiO_2NPs; synthesis of AgNPs-3MPS; experimental scheme for the evaluation of antibacterial activity; illumination setup for the EPR experiment; reaction scheme between TiO_2NPs−MPTMS and RHM; RHM calibration curve and UV−vis spectra of RHM stock solution and RHM supernatant after the interaction with TiO_2NPs−MPTMS; DLS and ζ-potential of TiO_2NPs−PEG; ATR-FTIR spectra of TiO_2NPs-PEG; FTIR ATR spectra of TiO_2NPs; ^{1}H NMR spectra of MPTMS and TiO_2NPs−MPTMS; XPS spectra of TiO_2NPs−MPTMS; FESEM and EDX images of TiO_2NP−Ag_4a; FTIR-ATR spectra of AgNPs-3MPS and TiO_2−Ag_4; XPS spectra of TiO_2−Ag_1; FESEM images and size distribution of TiO_2NPs at pH 3, 7, and 11; FESEM and EDX images of TiO_2NPs-MPTMS; LAE (% LAE) on AgNPs (pristine and aged), MPTMS, and PEG stabilized TiO_2NPs, TiO_2−Ag_4, TiO_2−Ag_1, and TiO_2NPs/AgNPs physical mix for *E. coli* and *S. aureus*; hydrodynamic ($\langle 2R_H \rangle$) stability over time in LB broth of TiO_2NPs-MPTMS, TiO_2−Ag_1, and TiO_2−Ag_4 nanohybrids; different reaction parameters for TiO_2NPs−MPTMS synthesis and DLS results; vibrational bands of pristine TiO_2NPs, free MPTMS, and functionalized TiO_2NPs−MPTMS; XPS data of TiO_2NPs−MPTMS; and XPS data of TiO_2−Ag_1 (PDF)

■ AUTHOR INFORMATION

Corresponding Authors

Martina Mercurio − *Department of Chemistry, Sapienza University of Rome, 00185 Rome, Italy*; Phone: 0039-06 4991 3352; Email: martina.mercurio@uniroma1.it

Ilaria Fratoddi − *Department of Chemistry, Sapienza University of Rome, 00185 Rome, Italy; Research Center for Applied Sciences to the Safeguard of Environment and*

https://doi.org/10.1021/acsanm.4c04409
ACS Appl. Nano Mater. XXXX, XXX, XXX−XXX

Cultural Heritage and Research Center for Nanotechnology Applied to Engineering of Sapienza, Sapienza University of Rome, 00185 Rome, Italy; orcid.org/0000-0002-5172-0636; Phone: 0039-06 4991 3182; Email: ilaria.fratoddi@uniroma1.it

Authors

Farid Hajareh Haghighi − *Department of Chemistry, Sapienza University of Rome, 00185 Rome, Italy*

Francesca Ubaldi − *Department of Movement, Health and Human Sciences, University of Rome Foro Italico, 00135 Rome, Italy*

Sara Cerra − *Department of Chemistry, Sapienza University of Rome, 00185 Rome, Italy;* orcid.org/0000-0002-5549-9406

Maria Luisa Astolfi − *Department of Chemistry, Sapienza University of Rome, 00185 Rome, Italy;* orcid.org/0000-0001-9633-8484

Roberto Matassa − *Physics Division, School of Science and Technology, University of Camerino, 62032 Camerino, Macerata, Italy;* orcid.org/0000-0002-6336-4587

Chiara Battocchio − *Department of Sciences, Roma Tre University, 00146 Rome, Italy;* orcid.org/0000-0003-4590-0865

Martina Marsotto − *Department of Chemical Sciences and Technologies, University of Rome, Tor Vergata, Rome 00133, Italy*

Cinzia De Angelis − *Istituto Superiore di Sanità, Rome 00161, Italy*

Sara Della Monaca − *Istituto Superiore di Sanità, Rome 00161, Italy*

Paola Fattibene − *Istituto Superiore di Sanità, Rome 00161, Italy*

Federica Valeriani − *Department of Movement, Health and Human Sciences, University of Rome Foro Italico, 00135 Rome, Italy*

Vincenzo Romano Spica − *Department of Movement, Health and Human Sciences, University of Rome Foro Italico, 00135 Rome, Italy*

Complete contact information is available at: https://pubs.acs.org/10.1021/acsanm.4c04409

Notes

The authors declare no competing financial interest.

■ ACKNOWLEDGMENTS

The authors gratefully acknowledge for the financial support Sapienza funding grant Ateneo Ricerca 2022 (RM1221867C322C1). The authors acknowledge financial support from the National Quantum Science Technology Institute within PNRR MUR project PE0000023-NQSTI. The authors are grateful to the Advanced Microscopy Laboratory (AML) in CRANN for the provision of their facilities and expertise, Trinity College Dublin, Ireland. This study was partially funded by the MIUR-Fund-PON R&I 2014−2020 React-EU and "Foro Italico" Project [CUP H83C23000160001].

■ REFERENCES

(1) Younis, A. B.; Haddad, Y.; Kosaristanova, L.; Smerkova, K. Titanium Dioxide Nanoparticles: Recent Progress in Antimicrobial Applications. *Wiley Interdiscip. Rev.: Nanomed. Nanobiotechnol.* **2023**, *15*, e1860.

(2) Lofrano, G.; Ubaldi, F.; Albarano, L.; Carotenuto, M.; Vaiano, V.; Valeriani, F.; Libralato, G.; Gianfranceschi, G.; Fratoddi, I.; Meric, S.; Guida, M.; Romano Spica, V. Antimicrobial Effectiveness of Innovative Photocatalysts: A Review. *Nanomaterials* **2022**, *12* (16), 2831.

(3) Hajareh Haghighi, F.; Mercurio, M.; Cerra, S.; Salamone, T. A.; Bianymotlagh, R.; Palocci, C.; Romano Spica, V.; Fratoddi, I. Surface Modification of TiO_2 Nanoparticles with Organic Molecules and Their Biological Applications. *J. Mater. Chem. B* **2023**, *11* (11), 2334−2366.

(4) Hasanzadeh Kafshgari, M.; Goldmann, W. H. Insights into Theranostic Properties of Titanium Dioxide for Nanomedicine. *Nano-Micro Lett.* **2020**, *12* (1), 22.

(5) Yang, T.; Qian, S.; Qiao, Y.; Liu, X. Cytocompatibility and Antibacterial Activity of Titania Nanotubes Incorporated with Gold Nanoparticles. *Colloids Surf., B* **2016**, *145*, 597−606.

(6) Albert, E.; Albouy, P. A.; Ayral, A.; Basa, P.; Csík, G.; Nagy, N.; Roualdès, S.; Rouessac, V.; Sáfrán, G.; Suhajda, A. ·.; Zolnai, Z.; Hórvölgyi, Z. Antibacterial Properties of Ag−TiO_2 Composite Sol−Gel Coatings. *RSC Adv.* **2015**, *5* (73), 59070−59081.

(7) Schutte-Smith, M.; Erasmus, E.; Mogale, R.; Marogoa, N.; Jayiya, A.; Visser, H. G. Using Visible Light to Activate Antiviral and Antimicrobial Properties of TiO_2 Nanoparticles in Paints and Coatings: Focus on New Developments for Frequent-Touch Surfaces in Hospitals. *J. Coat. Technol. Res.* **2023**, *20*, 789−817.

(8) Margarucci, L. M.; Gianfranceschi, G.; Romano Spica, V.; D'Ermo, G.; Refi, C.; Podico, M.; Vitali, M.; Romano, F.; Valeriani, F. Photocatalytic Treatments for Personal Protective Equipment: Experimental Microbiological Investigations and Perspectives for the Enhancement of Antimicrobial Activity by Micrometric TiO_2. *Int. J. Environ. Res. Public Health* **2021**, *18* (16), 8662.

(9) Deshmukh, S. P.; Patil, S. M.; Mullani, S. B.; Delekar, S. D. Silver Nanoparticles as an Effective Disinfectant: A Review. *Mater. Sci. Eng., C* **2019**, *97*, 954−965.

(10) Luceri, A.; Francese, R.; Lembo, D.; Ferraris, M.; Balagna, C. Silver Nanoparticles: Review of Antiviral Properties, Mechanism of Action and Applications. *Microorganisms* **2023**, *11* (3), 629.

(11) Anees Ahmad, S.; Sachi Das, S.; Khatoon, A.; Tahir Ansari, M.; Afzal, M.; Saquib Hasnain, M.; Kumar Nayak, A. Bactericidal Activity of Silver Nanoparticles: A Mechanistic Review. *Mater. Sci. Energy Technol.* **2020**, *3*, 756−769.

(12) Mikhailova, E. O. Silver Nanoparticles: Mechanism of Action and Probable Bio-Application. *J. Funct. Biomater.* **2020**, *11* (4), 84.

(13) Fratoddi, I.; Battocchio, C.; Iucci, G.; Catone, D.; Cartoni, A.; Paladini, A.; O'Keeffe, P.; Nappini, S.; Cerra, S.; Venditti, I. Silver Nanoparticles Functionalized by Fluorescein Isothiocyanate or Rhodamine B Isothiocyanate: Fluorescent and Plasmonic Materials. *Appl. Sci.* **2021**, *11* (6), 2472.

(14) Chhatre, A.; Solasa, P.; Sakle, S.; Thaokar, R.; Mehra, A. Color and Surface Plasmon Effects in Nanoparticle Systems: Case of Silver Nanoparticles Prepared by Microemulsion Route. *Colloids Surf., A* **2012**, *404*, 83−92.

(15) Frei, A.; Verderosa, A. D.; Elliott, A. G.; Zuegg, J.; Blaskovich, M. A. T. Metals to Combat Antimicrobial Resistance. *Nat. Rev. Chem* **2023**, *7* (3), 202−224.

(16) Butler, J.; Handy, R. D.; Upton, M.; Besinis, A. Review of Antimicrobial Nanocoatings in Medicine and Dentistry: Mechanisms of Action, Biocompatibility Performance, Safety, and Benefits Compared to Antibiotics. *ACS Nano* **2023**, *17* (8), 7064−7092.

(17) Wang, J.; Svoboda, L.; Němečková, Z.; Sgarzi, M.; Henych, J.; Licciardello, N.; Cuniberti, G. Enhanced Visible-Light Photodegradation of Fluoroquinolone-Based Antibiotics and *E. Coli* Growth Inhibition Using Ag−TiO_2 Nanoparticles. *RSC Adv.* **2021**, *11* (23), 13980−13991.

(18) Abdulkadhim, W. K. Synthesis Titanium Dioxide Nanoparticles Doped with Silver and Novel Antibacterial Activity. *J. Phys.: Conf. Ser.* **2021**, *1999* (1), 012033.

(19) Hérault, N.; Wagner, J.; Abram, S.-L.; Widmer, J.; Horvath, L.; Vanhecke, D.; Bourquin, C.; Fromm, K. M. Silver-Containing

Titanium Dioxide Nanocapsules for Combating Multidrug-Resistant Bacteria. *Int. J. Nanomed.* **2020**, *15*, 1267−1281.
(20) Nguyen, V. T.; Tabish, M.; Yasin, G.; Bilal, M.; Nguyen, T. H.; Van, C. P.; Nguyen-Tri, P.; Gupta, R. K.; Nguyen, T. A. A Facile Strategy for the Construction of TiO2/Ag Nanohybrid-Based Polyethylene Nanocomposite for Antimicrobial Applications. *Nano-Struct. Nano-Objects* **2021**, *25*, 100671.
(21) Oliani, W. L.; Pusceddu, F. H.; Parra, D. F. Silver-Titanium Polymeric Nanocomposite Non Ecotoxic with Bactericide Activity. *Polym. Bull.* **2022**, *79* (12), 10949−10968.
(22) Zafar, N.; Uzair, B.; Niazi, M. B. K.; Samin, G.; Bano, A.; Jamil, N.; Waqar-Un-Nisa; Sajjad, S.; Menaa, F. Synthesis and Characterization of Potent and Safe Ciprofloxacin-Loaded Ag/TiO_2/CS Nanohybrid against Mastitis Causing *E. Coli*. *Crystals* **2021**, *11* (3), 319.
(23) Coman, A. N.; Mare, A.; Tanase, C.; Bud, E.; Rusu, A. Silver-Deposited Nanoparticles on the Titanium Nanotubes Surface as a Promising Antibacterial Material into Implants. *Metals* **2021**, *11* (1), 92.
(24) Sun, L.; Chen, X.; Chen, R.; Ji, Z.; Mu, H.; Liu, C.; Yu, J.; Wang, J.; Xia, R.; Zhang, S.; Xu, Y.; Ma, K.; Xia, L. Balancing the Antibacterial and Osteogenic Effects of Double-Layer TiO_2 Nanotubes Loaded with Silver Nanoparticles for the Osseointegration of Implants. *Nanoscale* **2023**, *15* (6), 2911−2923.
(25) Soo, J. Z.; Chai, L. C.; Ang, B. C.; Ong, B. H. Enhancing the Antibacterial Performance of Titanium Dioxide Nanofibers by Coating with Silver Nanoparticles. *ACS Appl. Nano Mater.* **2020**, *3* (6), 5743−5751.
(26) Tobaldi, D. M.; Piccirillo, C.; Pullar, R. C.; Gualtieri, A. F.; Seabra, M. P.; Castro, P. M. L.; Labrincha, J. A. Silver-Modified Nano-Titania as an Antibacterial Agent and Photocatalyst. *J. Phys. Chem. C* **2014**, *118* (9), 4751−4766.
(27) Meng, L.; Liu, Z.; Lan, C.; Xu, N. In-Situ Fabricating Ag Nanoparticles on TiO2 for Unprecedented High Catalytic Activity of 4-Nitrophenol Reduction. *Catal. Lett.* **2022**, *152* (3), 912−920.
(28) Stöber, W.; Fink, A.; Bohn, E. Controlled Growth of Monodisperse Silica Spheres in the Micron Size Range. *J. Colloid Interface Sci.* **1968**, *26* (1), 62−69.
(29) Pallavicini, P.; Cabrini, E.; Casu, A.; Dacarro, G.; Antonio Diaz-Fernandez, Y.; Falqui, A.; Milanese, C.; Vita, F. Silane-Coated Magnetic Nanoparticles with Surface Thiol Functions for Conjugation with Gold Nanostars. *Dalton Trans.* **2015**, *44* (48), 21088−21098.
(30) Astolfi, M. L.; Marconi, E.; Vitiello, G.; Massimi, L. An Optimized Method for Sample Preparation and Elemental Analysis of Extra-Virgin Olive Oil by Inductively Coupled Plasma Mass Spectrometry. *Food Chem.* **2021**, *360*, 130027.
(31) Reina, G.; Tamburri, E.; Orlanducci, S.; Gay, S.; Matassa, R.; Guglielmotti, V.; Lavecchia, T.; Letizia Terranova, M.; Rossi, M. Nanocarbon Surfaces for Biomedicine. *Biomatter* **2014**, *4* (1), No. e28537.
(32) Rathod, P. B.; Waghuley, S. A. Synthesis and UV-Vis Spectroscopic Study of TiO_2 Nanoparticles. *Int. J. Nanomanuf.* **2015**, *11* (3/4), 185−193.
(33) Nagao, Y.; Yoshikawa, A.; Koumoto, K.; Kato, T.; Ikuhara, Y.; Ohta, H. Experimental Characterization of the Electronic Structure of Anatase TiO_2: Thermopower Modulation. *Appl. Phys. Lett.* **2010**, *97* (17), 172112.
(34) Wang, C.; Li, J.; Mele, G.; Duan, M.; Lü, X. f.; Palmisano, L.; Vasapollo, G.; Zhang, F. The Photocatalytic Activity of Novel, Substituted Porphyrin/TiO_2-Based Composites. *Dyes Pigm.* **2010**, *84* (2), 183−189.
(35) Kassir, M.; Roques-Carmes, T.; Hamieh, T.; Toufaily, J.; Akil, M.; Barres, O.; Villiéras, F. Improvement of the Photocatalytic Activity of TiO_2 Induced by Organic Pollutant Enrichment at the Surface of the Organografted Catalyst. *Colloids Surf., A* **2015**, *485*, 73−83.
(36) Bhattacharjee, S. DLS and Zeta Potential − What They Are and What They Are Not? *J. Controlled Release* **2016**, *235*, 337−351.
(37) Avram, M.; Mateescu, G. H. Chapter 10: Carbohydrates in Infrared Spectroscopy. *Applications in Organic Chemistry*, 2nd ed.; R. E. Krieger Publishing Company: Huntington, NY, 1978.
(38) Arkles, B.; Larson, G. L. *Silicon Compounds: Silanes and Silicones*, 3 ed.; Gelest: Morrisville, PA, 2013.
(39) Lihitkar, N. B.; Abyaneh, M. K.; Samuel, V.; Pasricha, R.; Gosavi, S. W.; Kulkarni, S. K. Titania Nanoparticles Synthesis in Mesoporous Molecular Sieve MCM-41. *J. Colloid Interface Sci.* **2007**, *314*, 310−316.
(40) Al-Amin, M.; Dey, S. C.; Rashid, T. U.; Ashaduzzaman, M.; Shamsuddin, S. M. Solar Assisted Photocatalytic Degradation of Reactive Azo Dyes in Presence of Anatase Titanium Dioxide. *Int. J. Latest Res. Eng. Technol.* **2016**, *2*, 14−21.
(41) Tan, D.; Ma, Z.; Xu, B.; Dai, Y.; Ma, G.; He, M.; Jin, Z.; Qiu, J. Surface Passivated Silicon Nanocrystals with Stable Luminescence Synthesized by Femtosecond Laser Ablation in Solution. *Phys. Chem. Chem. Phys.* **2011**, *13* (45), 20255.
(42) Sahasrabudhe, G.; Rupich, S. M.; Jhaveri, J.; Berg, A. H.; Nagamatsu, K. A.; Man, G.; Chabal, Y. J.; Kahn, A.; Wagner, S.; Sturm, J. C.; Schwartz, J. Low-Temperature Synthesis of a TiO_2/Si Heterojunction. *J. Am. Chem. Soc.* **2015**, *137* (47), 14842−14845.
(43) Zhang, S.; Zhang, Y.; Liu, J.; Xu, Q.; Xiao, H.; Wang, X.; Xu, H.; Zhou, J. Thiol Modified Fe_3O_4@SiO_2 as a Robust, High Effective, and Recycling Magnetic Sorbent for Mercury Removal. *Chem. Eng. J.* **2013**, *226*, 30−38.
(44) Zhang, Y.; Xu, Q.; Zhang, S.; Liu, J.; Zhou, J.; Xu, H.; Xiao, H.; Li, J. Preparation of Thiol-Modified Fe_3O_4@SiO_2 Nanoparticles and Their Application for Gold Recovery from Dilute Solution. *Sep. Purif. Technol.* **2013**, *116*, 391−397.
(45) Grabowska, E.; Zaleska, A.; Sorgues, S.; Kunst, M.; Etcheberry, A.; Colbeau-Justin, C.; Remita, H. Modification of Titanium(IV) Dioxide with Small Silver Nanoparticles: Application in Photocatalysis. *J. Phys. Chem. C* **2013**, *117* (4), 1955−1962.
(46) Elim, H. I.; Cai, B.; Kurata, Y.; Sugihara, O.; Kaino, T.; Adschiri, T.; Chu, A.-L.; Kambe, N. Refractive Index Control and Rayleigh Scattering Properties of Transparent TiO_2 Nanohybrid Polymer. *J. Phys. Chem. B* **2009**, *113*, 10143−10148.
(47) Bradley, Z.; Cunningham, D.; Bhalla, N. Refractive Index-Modulated LSPR Sensing in 20−120 Nm Gold and Silver Nanoparticles: A Simulation Study. *ECS Sens. Plus* **2023**, *2*, 043402.
(48) Liu, X.; Luo, Y.; Wu, T.; Huang, J. Antibacterial Activity of Hierarchical Nanofibrous Titania−Carbon Composite Material Deposited with Silver Nanoparticles. *New J. Chem.* **2012**, *36*, 2568.
(49) Pan, X.; Medina-Ramirez, I.; Mernaugh, R.; Liu, J. Nano-characterization and Bactericidal Performance of Silver Modified Titania Photocatalyst. *Colloids Surf., B* **2010**, *77*, 82−89.
(50) Adams, D. M.; Cornell, J. B. Metal−Sulphur Vibrations. Part I. Far-Infrared Spectra of Some Complexes of Thiourea and Ethylenethiourea (Imidazolidine-2-Thione). *J. Chem. Soc. A* **1967**, *0* (0), 884−889.
(51) Secchi, V.; Franchi, S.; Dettin, M.; Zamuner, A.; Beranová, K.; Vladescu, A.; Battocchio, C.; Graziani, V.; Tortora, L.; Iucci, G. Hydroxyapatite Surfaces Functionalized with a Self-Assembling Peptide: XPS, RAIRS and NEXAFS Study. *Nanomaterials* **2020**, *10* (6), 1151.
(52) Mochi, F.; Burratti, L.; Fratoddi, I.; Venditti, I.; Battocchio, C.; Carlini, L.; Iucci, G.; Casalboni, M.; De Matteis, F.; Casciardi, S.; Nappini, S.; Pis, I.; Prosposito, P. Plasmonic Sensor Based on Interaction between Silver Nanoparticles and Ni^{2+} or Co^{2+} in Water. *Nanomaterials* **2018**, *8* (7), 488.
(53) Hajareh Haghighi, F.; Mercurio, M.; Cerra, S.; Palocci, C.; Rossi, M.; Marsotto, M.; Battocchio, C.; Fratoddi, I. Direct Conjugation of TiO_2 Nanoparticles with Phototherapeutic Prodrug 5-Aminolevulinic Acid. *ChemNanoMat* **2024**, *10*, No. e202400310.
(54) Kraleva, E.; Saladino, M. L.; Matassa, R.; Caponetti, E.; Enzo, S.; Spojakina, A. Phase Formation in Mixed TiO_2-ZrO_2 Oxides Prepared by Sol-Gel Method. *J. Struct. Chem.* **2011**, *52* (2), 330−339.

https://doi.org/10.1021/acsanm.4c04409
ACS Appl. Nano Mater. XXXX, XXX, XXX−XXX

(55) Djerdj, I.; Tonejc, A. M. Structural Investigations of Nanocrystalline TiO_2 Samples. *J. Alloys Compd.* **2006**, *413* (1−2), 159−174.
(56) Frueh, A. J. The Crystallography of Silver Sulfide, Ag_2S. *Z. Kristallogr. Cryst. Mater.* **1958**, *110* (1−6), 136−144.
(57) Chiesa, M.; Giamello, E.; Livraghi, S.; Paganini, M. C.; Polliotto, V.; Salvadori, E. Electron Magnetic Resonance in Heterogeneous Photocatalysis Research. *J. Phys.: Condens. Matter* **2019**, *31*, 444001.
(58) Taglietti, A.; Diaz Fernandez, Y. A.; Amato, E.; Cucca, L.; Dacarro, G.; Grisoli, P.; Necchi, V.; Pallavicini, P.; Pasotti, L.; Patrini, M. Antibacterial Activity of Glutathione-Coated Silver Nanoparticles against Gram Positive and Gram-Negative Bacteria. *Langmuir* **2012**, *28* (21), 8140−8148.
(59) Nguyen, V.; Vu, V.; Nguyen, T.; Nguyen, T.; Tran, V.; Nguyen-Tri, P. Antibacterial Activity of TiO_2- and ZnO-Decorated with Silver Nanoparticles. *J. Compos. Sci.* **2019**, *3* (2), 61.
(60) Lungu, M.; Gavriliu, Ş.; Enescu, E.; Ion, I.; Brătulescu, A.; Mihăescu, G.; Măruţescu, L.; Chifiriuc, M. C. Silver−Titanium Dioxide Nanocomposites as Effective Antimicrobial and Antibiofilm Agents. *J. Nanopart. Res.* **2014**, *16* (1), 2203.
(61) Zhang, H.; Chen, G. Potent Antibacterial Activities of Ag/TiO_2 Nanocomposite Powders Synthesized by a One-Pot Sol−Gel Method. *Environ. Sci. Technol.* **2009**, *43*, 2905−2910.
(62) Prathna, T. C.; Chandrasekaran, N.; Mukherjee, A. Studies on aggregation behaviour of silver nanoparticles in aqueous matrices: Effect of surface functionalization and matrix composition. *Colloids Surf., A* **2011**, *390*, 216−224.

https://doi.org/10.1021/acsanm.4c04409
ACS Appl. Nano Mater. XXXX, XXX, XXX−XXX